Title
Characterization of synaptic inputs to transient ON/OFF amacrine cells in tiger salamander retina

Author
Hwang, Thomas Nyping

Publication Date
2000

Peer reviewed|Thesis/dissertation

Characterization of Synaptic Inputs to Transient ON/OFF Amacrine Cells

in Tiger Salamander Retina

by

Thomas Nyping Hwang

DISSERTATION

Submitted in partial satisfaction of the requirements for the degree of

DOCTOR OF PHILOSOPHY

in

Biomedical Sciences

in the

GRADUATE DIVISION

of the

UNIVERSITY OF CALIFORNIA SAN FRANCISCO

Date University Librarian

Degree Conferred: .....

Acknowledgements

I would like to thank my thesis advisor, Dr. David Copenhagen, for his contribution to this dissertation and my graduate school experience. I could not have asked for a better mentor to teach me about the scientific approach and doing academic research. His advice was invaluable both scientifically and personally. I consider myself incredibly fortunate to have him as a thesis advisor and friend.

My time as a graduate student would not have been nearly as enjoyable or instructive without the past and present members of the Copenhagen lab. These people include Dr. Ning Tian, Dr. Mark Bieda, Dr. David Krizaj, Dr. Tania Vu, Dr. Rene Renteria, and Dr. Juliette Johnson. Our many discussions together included topics ranging from scientific papers and experiments to the latest high-tech hardware and video games. I greatly appreciated their company and learned a great deal from each of them.

I owe a great deal of thanks to my thesis committee members, Dr. Julie Schnapf and Dr. Ken Miller, who were very patient with me as I struggled toward the completion of my dissertation. In addition, I would like to acknowledge that the work presented in the last chapter of my thesis has appeared in published form in the following reference: Hwang, TN and Copenhagen DR (1999). "Automatic detection, characterization, and discrimination of kinetically distinct spontaneous synaptic events." Journal of Neuroscience Methods 92(1-2):65-73.

I would also like to acknowledge my parents, Bruce and Shing Mei, for always supporting me in all my endeavors.

Finally, I need to mention the two most important people in my life, my wife Joyce and my daughter Jaclyn. Joyce has been an inspiration to me since the day I met her. Her faith in me and her love are amazing blessings that I never take for granted. As for Jaclyn, her smiling face, joyful laugh, and loving kisses and hugs somehow makes even the worst of days actually seem good.

Characterization of synaptic inputs to transient ON/OFF amacrine cells in tiger salamander retina

by

Thomas Nyping Hwang

This study examines excitatory and inhibitory synaptic transmission to transient ON/OFF amacrine cells using voltage clamp recordings in a tiger salamander retinal slice preparation. The experimental approach involves three different sections. In the first section, the presence of glycine, $GABA_A$, non-NMDA, and NMDA receptor-mediated spontaneous events are demonstrated and their respective kinetics quantified. In addition, for NMDA receptors, we provide the first evidence in an *in vivo* system that the receptors are mobile on the plasma membrane.

In the second section, we examine the presynaptic release of glycine, GABA, and glutamate onto amacrine cells. Our results show that voltage-gated sodium channels play a role in the spontaneous multi-quantal release of glycine and GABA but not glutamate. In contrast, blocking the voltage-gated calcium channel decreased the rate of multi-quantal release of all three neurotransmitters. Additional results on evoked responses show that maximum light responses involve the release of a few thousand quanta of glycine, GABA, and glutamate. For glutamate release, this number of quanta is many-fold less than the number of vesicles seen on synaptic ribbons in bipolar cells, suggesting

that light-evoked depletion of synaptic terminals is unlikely. This hypothesis is supported by the results of paired flash experiments.

In the third section, we focus on the circuitry underlying the release of glutamate from bipolar cells onto amacrine cells. Our findings show that a majority of the spontaneous glutamatergic input arises from ON-type rather than OFF-type bipolar cells. In addition, we demonstrate an inhibitory pathway via $GABA_C$ receptors that inhibits light-evoked and spontaneous release of glutamate from both ON and OFF bipolar cells.

As a tool for analyzing the spontaneous events, a computer program was created using a novel algorithm. Here, we describe and characterize an amplitude threshold algorithm, which detects events and characterizes their amplitudes and kinetics. Furthermore, if a recording has two kinetically-distinguishable types of events, the program can separate the events based on kinetics. In addition to using the program for my studies of amacrine cell activity in tiger salamander, this program was used to characterize synaptic events in mouse retinal ganglion cells (Tian et al., 1998).

Table of Contents

List of Figures

General Introduction

Amacrine cells, inhibitory interneurons of the inner retina, play a pivotal role in signal processing of visual information yet little is known quantitatively about the synaptic inputs to these cells in intact retinal tissue. Synaptically, amacrine cells receive excitatory input from bipolar cells and inhibitory input from other amacrine cells. In turn, they provide inhibitory input to bipolar cells, ganglion cells and other amacrine cells. Functionally, the roles of amacrine cells in retinal processing are still being delineated. However, at present, it is recognized that amacrine cells are involved in several important aspects of retinal function. They have been shown to play a major part in establishing the directional selectivity of ganglion cells (He and Masland, 1997; Grzywacz et al., 1998). In mammalian retinae, rod bipolar cells contact ganglion cells via an amacrine cell pathway instead of synapsing directly onto ganglion cells themselves (Kolb, 1979). Temporally, amacrine cells have been shown to modulate the response transience of inner retinal cells (Werblin et al., 1988; Maguire et al., 1989; Lukasiewicz et al., 1994; Nirenberg and Meister, 1997; Zhang et al., 1997; Dong and Werblin, 1998; Roska et al., 1998; Bieda and Copenhagen, 2000). Spatially, there is evidence that amacrine cells participate in generating the surround organization at the ganglion cell level (Werblin, 1972; Werblin and Copenhagen, 1974; Thibos and Werblin, 1978; Cook and McReynolds, 1998). Despite their importance, little work has been done in intact retinal tissue on the synaptic inputs to these cells.

Amacrine cells form an incredibly diverse population in the retina. A study in mammalian retina documented twenty-two anatomically-distinct types of amacrine cells (MacNeil and Masland, 1998). However, from a functional perspective, amacrine cells can be divided into six basic classes based up their responses to steps of light. Cells that respond only at the start of the light step are known as ON-type. Cells that respond only at the termination of light are known as OFF-type. Cells that response both at the start and end of the step of light are known as ON/OFF-type. In each of these three classes, the cells can then be further separated into two groups based upon whether their responses are sustained or transient. In the tiger salamander retina, a study has shown that transient ON-responses will terminate within 600 ms even in the face of continuous light stimulation (Bieda and Copenhagen, 2000). Approximately 90% of amacrine cells in the salamander retina have been shown to be transient ON/OFF cells (Dixon and Copenhagen, 1992); therefore, this study focuses mainly on this type of amacrine cell.

To analyze synaptic transmission to amacrine cells, this project uses an experimental approach with three different scopes. The first stage focuses on postsynaptic issues by characterizing the receptors used to receive synaptic input. The second stage deals with neurotransmitter release from presynaptic terminals by looking at the occurrence of multi-quantal release and vesicle depletion. Finally, the third stage studies the circuitry of the excitatory synaptic input by comparing ON- versus OFF-bipolar cell inputs and how they are affected

by the GABAergic inhibitory feedback circuit. The rationales and background material for each of these three studies is included in each chapter.

General Methods

Salamander retinal slice preparation

Larval stage tiger salamanders (*Ambystoma tigrinum* from Charles D. Sullivan Co.) were maintained under a 12-hour light-dark cycle in 4 degrees Celsius water. The handling and maintenance of animals and tissue preparation met the National Institute of Health guidelines and were approved by the University of California, San Francisco, Committee on Animal Research. Under dim room light, the animals were decapitated and double-pithed, and the eyes were removed. Preparation of retinal slices was also done under dim room illumination, following the basic procedure previously described previously (Wu, 1987). We placed the retina with the photoreceptors facing the filter paper for slicing in order to have better access to the inner retina (Tian and Slaughter, 1995; Tian et al., 1998). 250-micron slices were cut and stored in a light-tight ice box. The air inside the box was kept humidified by bubbling oxygen through a beaker of distilled water using an airstone. For each experiment, a single retinal slice was mounted in a recording chamber, which was continuously perfused with extracellular solution from a gravity-driven perfusion system at a rate of 1-2 ml per minute. All experiments were done at room temperature inside a light-sealed, Faraday recording cage.

Solutions and pharmacology

The extracellular control solution contained (in mM) 110 NaCl, 2.5 KCl, 1.5 $CaCl_2$, 1.5 $MgCl_2$, 10 glucose and 5 N-2-hydroxyethylpiperazine-N'-2-ethanesulfonic acid (HEPES) hemi-sodium. The pH was adjusted to 7.8 with

NaOH. The osmolarity was approximately 240 mOsm. The pipette solution for perforated patch clamp experiments contained (in mM) 105 CsMethanesulfonate, 1 CaCl2, 1.5 MgCl2, 10 ethylene glycol-bis (β-aminoethyl ether)-N, N, N', N'-tetra-acetic acid (EGTA) , 10 HEPES hemi-sodium, and 5 glucose. The pH was adjusted to 7.4 with CsOH. The osmolarity was approximately 240 mOsm. At these concentrations, the reversal potential for chloride was approximately -80 mV. The stock solution of amphotericin B (Sigma) contained 25 mg of amphotericin B powder in 1 ml dimethylsulfoxide (DMSO). After 20 minutes of sonication, the stock was aliquoted and stored at –20 degrees Celsius. On each experimental day, 4 ul of amphotericin stock solution was added to 1 ml of pipette solution and vortexed so that the final concentration was 100 ug/ml (0.4% DMSO), All of the pharmacological compounds were dissolved into extracellular control solution and superfused through the recording chamber from a gravity-driven perfusion system at a rate of 1-2 ml per minute. The following pharmacological agents were used in this study: tetrodotoxin (TTX,SIGMA), $CdCl_2$ (Sigma), CNQX (Tocris), AP7 (Tocris), SR95535 (Tocris), and strychnine (Sigma).

Patch-clamp recordings

Retinal slices were visualized on an upright microscope (Zeiss Axioskop, Carl Zeiss, Oberkochen, Germany) using a x40 water immersion objective. The microscope light source was in the infrared range (>850 nm), and a CCD videocamera (MTI) was used to display the image on a black-and-white monitor. Patch pipettes were pulled from borosillicate glass (type 7052, Garner Glass,

Clarement, CA) on a Brown-Flaming horizontal puller (model P-80/PC, Sutter Instruments, CA). The electrode bath resistance ranged from 4 to 8 Mohms. For each experiment, an electrode was back-filled with Amphotericin-containing internal solution and immersed in the bath solution without using positive pressure. We did not find it necessary to tip-fill with Amphotericin-free solution. After forming the gigaseal, cells were held at -70 mV for perforation. Cell access was monitored every thirty seconds until a stable level was achieved (<70 Mohms after 20 min) and then monitored every 5-10 minutes during the course of the experiment. Recordings were made using an Axopatch 1B amplifier (Axon Instruments, Foster City, CA), an ITC-16 analog-to-digital board (Instrutech, Great Neck, N Y), and a Power Macintosh G3 running Pulse 8.11 (HEKA elektronik GmbH, Germany). All recordings were filtered at 1 kHz at the amplifier and acquired at 2 kHz.

Amacrine cells were identified by their location along the inner margin of the inner nuclear layer. All cells in this study had a sodium current of at least several hundred pA and ranged to well over 1 nA. The light response was determined by recording the response to a 2-second step generated by a red (620 nm) LED placed near the slice. All cells presented here responded with an inward current at -70 mV at both the start and end of the light step, which confirmed their identifies as ON/OFF type of amacrine cell.

Data analysis

The detection and characterization of spontaneous events was performed off-line using a Power Macintosh G3 running Igor Pro (Wavemetics, Lake

Oswego, OR). To greatly facilitate the analysis of spontaneous activity, an in-lab computer program written for Igor was used to automatically detect and characterize these events (Hwang and Copenhagen, 1999). Using the program, the frequency, amplitude and kinetics of glutamatergic, GABAergic, and glycinergic spontaneous events were determined. The parameters selected to characterize each type of event were the 10-90% rise time and the decay time constant of the mean event waveform determined for each recording trace. Pharmacological experiments showed that the GABAergic and glycinergic events could easily be distinguished kinetically from the glutamatergic events by their reversal potentials and markedly slower decay times (Tian et al., 1998). As done in previous studies (Otis et al., 1991; Cohen et al., 1992; Manabe et al., 1992; Tian et al., 1998), , we applied the Kolmogorov-Smirnov (K-S) test to compare two amplitude distributions because it does not depend on the distributions being normal. The statistics software Statview was used to implement the K-S test, and the critical value used to determine whether two distributions were different was p=0.01.

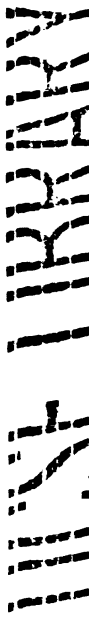

Chapter 1

Characterization of postsynaptic receptors mediating synaptic inputs to ON/OFF amacrine cells

Introduction

As a foundation for understanding the fundamental characteristics of amacrine cells, this study examines the synaptic inputs to these cells by characterizing the spontaneous synaptic activity and the light-driven responses in these cells. The excitatory input to amacrine cells comes from bipolar cells, which are non-spiking cells and which release glutamate. In neotenous tiger salamander, 90% of amacrine cells are transient ON/OFF cells (Dixon and Copenhagen, 1992), which depolarize briefly both at the start and end of a step of light. Recordings in tiger salamander have shown that, for these cells, the postsynaptic response to bipolar cell glutamatergic input can be mediated by both N-methyl-D-aspartate (NMDA) receptors and non-NMDA receptors (alpha-amino-3-hydroxy-5--methyl-4-isoxalole-4-propionic acid (AMPA) and/or kainate) (Dixon and Copenhagen, 1992). The inhibitory input originates from other amacrine cells, which release gamma-aminobutyric acid (GABA) or glycine onto their respective postsynaptic receptors. Application of antagonists to glycine and $GABA_A$ receptors showed that these two receptor types seem to mediate all the inhibitory input (Dixon and Copenhagen, 1992).

In many cases, neurons randomly release neurotransmitter, which can be recorded in postsynaptic cells as spontaneous postsynaptic currents (sPSCs).

In retinal ganglion cells, the kinetics of these events can be used to differentiate between various classes of synaptic inputs. We applied this same strategy to characterize the different synaptic inputs to amacrine cells. Previous work has demonstrated that the synaptic transmission from a presynaptic cell to two different classes of postsynaptic cells can have very different characteristics (Markram et al., 1998). Consequently, one of the primary goals of this study is to compare the kinetics of the synaptic inputs to amacrine and ganglion cells.

Results

Amacrine cell glycine and $GABA_A$ receptors have similar kinetics

Dixon and Copenhagen (1992) reported that the reversal potential for the excitatory input into amacrine cells was between 0 and +10 mV. Consequently, glycinergic events were recorded at +10 mV to isolate the inhibitory events while perfusing 10 μM SR95535, a specific $GABA_A$ receptor antagonist. Reversal of excitatory postsynaptic currents was verified for each cell. Fig 1.1A shows that SR95535 blocked a certain fraction of the inhibitory spontaneous activity recorded at +10mV, which were presumably the GABAergic events. Consistent with the remaining events being glycine-mediated, strychnine (1 uM), a specific glycine receptor antagonist, blocked all remaining spontaneous activity. Fig 1.1B shows a few examples of individual glycinergic events while Fig 1.1C shows the average waveform of all events detected from a single amacrine cell. The mean 10-90% rise time for the average glycinergic IPSCs (glyIPSCs) from all cells was 2.71 ± 0.68 ms (mean ± SD, # cells =17, # events = 5967) while the mean mono-exponential decay time constant was 20.68 ± 8.84 ms (mean ± SD, # cells =17, # events = 5967). Fig 1.1D shows that glycinergic events were distinguishable from the background noise by comparing the amplitude distribution of detected glycinergic events and the all-points distribution of a two second event-free segment of data. Fig 1.1E and F show the histograms for the 10-90% rise times and the decay time constants for the events respectively. Both of these distributions are unimodal, consistent with the presence of only one kinetically distinguishable type of event.

Fig 1.1: Kinetics of glycine receptor-mediated spontaneous events. Spontaneous inhibitory synaptic events were recorded from a voltage-clamped ON/OFF amacrine cell (Cs-methanesulfonate internal solution). The holding potential was +10 mV which was the effective reversal potential for excitatory currents. A) The top trace shows a ten second segment of spontaneous activity in external control solution. The middle trace shows that SR95535 (10 uM) blocked some of the activity. The bottom trace shows that strychnine (1 uM) blocked the remaining activity, demonstrating that the SR95535 (10 uM) effectively isolated glycinergic events. B) Examples of spontaneous synaptic events taken from the middle trace shown in panel A. C) The mean event waveform averaged from all events had a 10-90% rise time of 2.82 ms and a mono-exponential decay time constant of 19.9 ms (# events = 843). D) The open bars show the amplitude distribution of the events from the middle trace in panel A. The solid bars show the all-points histogram of a 2 second event free segment of the same trace scaled to match the peak of the event amplitude distribution shown by the open bars. This graph reveals that our selected amplitude criteria was sufficient to minimize effects from background noise. E) The bar graph of the 10-90% rise time distribution had a single mode at approximately 2.5 ms. F) The bar graph of the mono-exponential decay time constant had a single mode at approximately 18 ms.

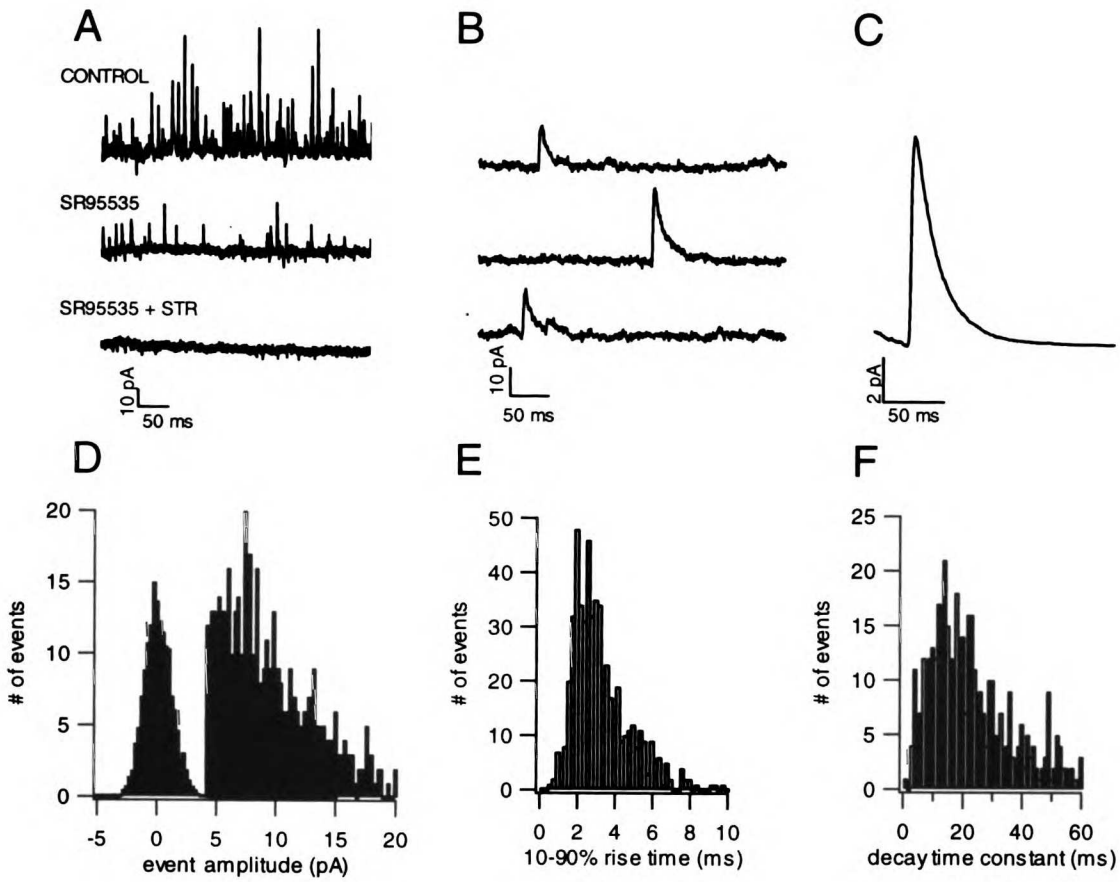

The decay phase of spontaneous IPSCs has been described either by a single or a double exponential curve (Gao and Wu, 1998; Tian et al., 1998; Protti et al., 2000). Using the adjusted R^2 statistic to compare the single and double exponential fits of each event showed that 21.1 ± 7.2% (mean ± SD, # cells =17, # events = 5967) of the events were significantly better fit with a bi-exponential curve. Visual inspection verified the biphasic decay of these events. This percentage is comparable to the percentage found in mouse using the same criteria . As mentioned above, fitting a single exponential curve to the mean glyIPSCs resulted in a mean decay time constant of 20.68 ± 8.84 ms (mean ± SD, # cells =17, # events = 5967). In contrast, those events that were fit significantly better by a double exponential resulted in mean time constants of 2.64 ± 1.36 ms and 28.50 ± 13.25 ms (mean ± SD, # cells =17, # events = 5967). These values do not resemble the values of 12.4 and 386.1 ms reported for glycinergic events in ganglion cells in tiger salamander (Gao and Wu, 1998). This discrepancy may be a result of different glycinergic receptor subunit composition in amacrine and ganglion cells. However, fitting data with a bi-exponential curve is highly sensitive to many factors, including selection of the starting and ending point for the fit. Consequently, the discrepancy could also result from differences in analysis. In addition, the recording conditions were slightly different, in particular in terms of the pH of the internal and external solutions used, which also might affect observed kinetics.

We isolated GABAergic events by holding cells at +10 mV to isolate the inhibitory event while perfusing the slice with 1 μM strychnine, a glycinergic

antagonist. Fig 1.2A shows that strychnine blocked some of the activity and that SR95535 then blocked the remaining activity. Individual examples of GABAergic events are shown in Fig 1.2B. The average waveform of the events shows that the kinetics of GABAergic events resemble those of glycinergic events (Fig 1.2C). For this cell, the 10-90% rise time of this was 2.48 ms and the single exponential decay time constant was 20.4 ms (# events = 433). Fig 1.2D shows the amplitude histogram of detected events compared to the all-points histogram of a two second event-free segment of data. The events were distinguishable from the background noise. Fig 1.2E and F show the histograms of the 10-90% rise time and the mono-exponential decay time constant for the detected events respectively. Both of these distributions are unimodal, consistent with the presence of only one kinetically distinguishable type of event.

Averaged over all cells, the 10-90% rise time was 2.96 ± 1.40 ms and the single exponential decay time constant was 22.67 ± 7.12 ms (mean ± SD, # cells = 25, # events = 4813). The adjusted R^2 test showed that 25.6 ± 7.3% (mean ± SD, # cells = 25, # events = 4813) of all detected GABA events was significantly better fit with a double exponential curve. Visual inspection revealed that the events isolated did appear to have biphasic decay. Including only those events that were classified as better fit with a double exponential yielded average decay time constants of 3.05 ± 1.33 ms and 48.49 ± 24.90 ms (mean ± SD, # cells = 25, # events = 4813). Similar to the glycinergic events, neither of these sets of values is very similar to the values of 10.5 and 89.5 ms reported for GABAergic events in ganglion cells in salamander (Gao and Wu, 1998). Again, this

Fig 1.2: Kinetics of $GABA_A$ receptor-mediated spontaneous events. Spontaneous excitatory synaptic events were recorded from a voltage-clamped ON/OFF amacrine cell (Cs-methanesulfonate internal solution). The holding potential was +10 mV which was the effective reversal potential for inhibitory currents. A) The top trace shows a ten second segment of spontaneous activity in external control solution. The middle trace shows that strychnine (1 uM) blocked some of the activity. The bottom trace shows that SR95535 (10 uM) blocked the remaining activity, demonstrating that the strychnine (1 uM) effectively isolated glycinergic events. B) Examples of spontaneous synaptic events taken from the middle trace shown in panel A. C) The mean event waveform averaged from all events had a 10-90% rise time of 2.42 ms and a mono-exponential decay time constant of 20.4 ms (# events = 433). D) The open bars show the amplitude distribution of the events from the middle trace in panel A. The solid bars show the all-points histogram of a 2 second event free segment of the same trace scaled to match the peak of the event amplitude distribution shown by the open bars. This graph reveals that the events were distinguishable from the background noise. E) The bar graph of the 10-90% rise time distribution had a single mode at approximately 2.5 ms. F) The bar graph of the mono-exponential decay time constant had a single mode at approximately 14 ms.

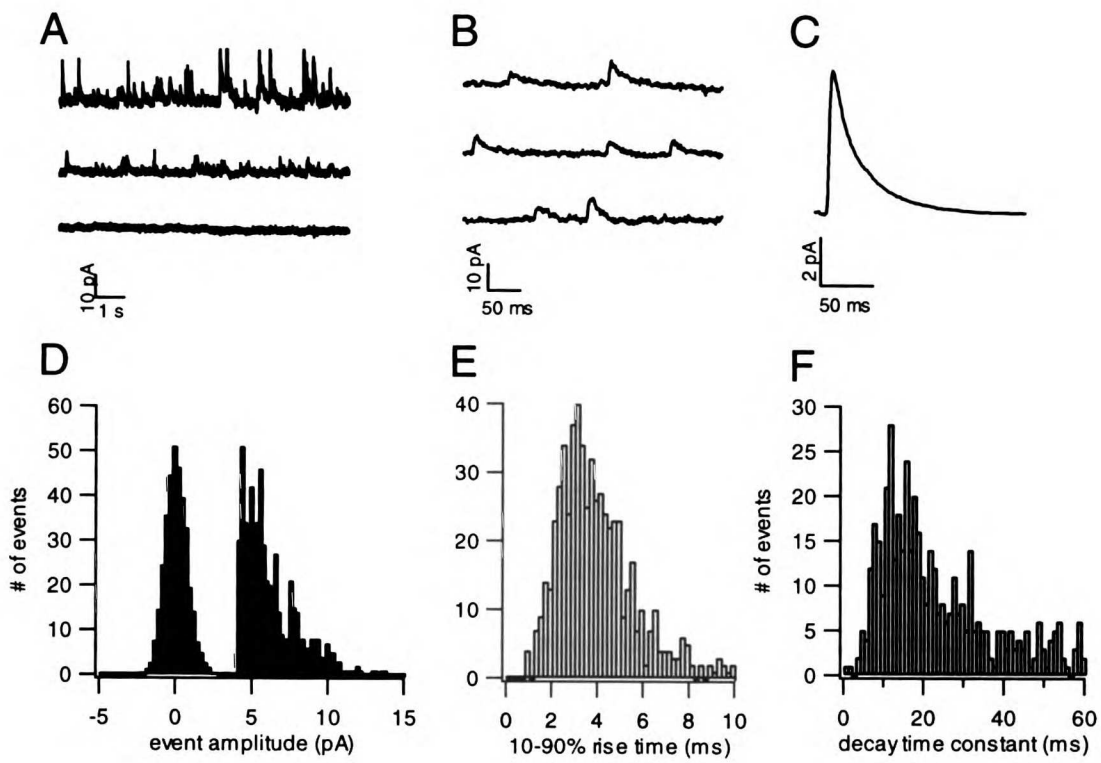

discrepancy may be a result of differences in $GABA_A$ receptor subunit composition in amacrine and ganglion cells, differences in the curve-fitting analysis, or differences in recording conditions.

Spontaneous non-NMDA events have fast kinetics and are mediated by AMPA receptors

To isolate spontaneous excitatory postsynaptic currents (sEPSCs), we recorded membrane currents at -70 mV, near the calculated chloride reversal potential for our recording solutions. As shown in Fig 1.3A, sEPSCs appeared as brief inward currents, which were blocked by non-NMDA receptor antagonist CNQX. Dixon and Copenhagen (1992) showed that transient amacrine cells light responses do have an NMDA-mediated component, however NMDA receptor-mediated spontaneous events would be virtually undetectable because NMDA-mediated currents would be strongly blocked by Mg^{2+} at –70 mV. Fig 1.3B shows several short recording segments to illustrate examples of the spontaneous events. The average event waveform (Fig 1.3C) reveals the fast kinetics of the non-NMDA mediated events. In this cell, the 10-90% rise time was 0.91 ms and the decay time constant was 4.21 ms (# events = 2500). Fig 1.3D plots the amplitude histogram of detected events (open bars) as well as an all-points histogram of a two second event-free recording segment (filled bars). Comparison of the two histograms shows that events detected were easily distinguishable from the background noise. Fig 1.3E and F plot the histograms of the rise time and mono-exponentially-fitted decay time constant of detected events, respectively. Both of these distributions are unimodal, consistent with the

Fig 1.3: Kinetics of non-NMDA receptor-mediated spontaneous events. Spontaneous excitatory synaptic events were recorded from a voltage-clamped ON/OFF amacrine cell (Cs-methanesulfonate internal solution). The holding potential was -70 mV, which was the effective reversal potential for inhibitory currents. A) The top trace shows a ten second segment of spontaneous activity in external control solution. The middle trace shows that CNQX (2 μM) blocked all activity. The third trace shows that the inhibition by CNQX was reversible. B) Examples of spontaneous synaptic events taken from the top trace shown in panel A. C) The mean event waveform averaged from all events had a 10-90% rise time of 0.91 ms and a mono-exponential decay time constant of 4.21 ms (# events = 2500). D) The open bars show the amplitude distribution of the events from the top trace in panel A. The solid bars show the all-points histogram of a 2 second event free segment of the same trace scaled to match the peak of the event amplitude distribution shown by the open bars. This graph reveals that the events were distinguishable from the background noise. E) The bar graph of the 10-90% rise time distribution of the events shows a single mode at approximately 1 ms. F) The bar graph of the mono-exponential decay time constant shows a single mode at approximately 4 ms.

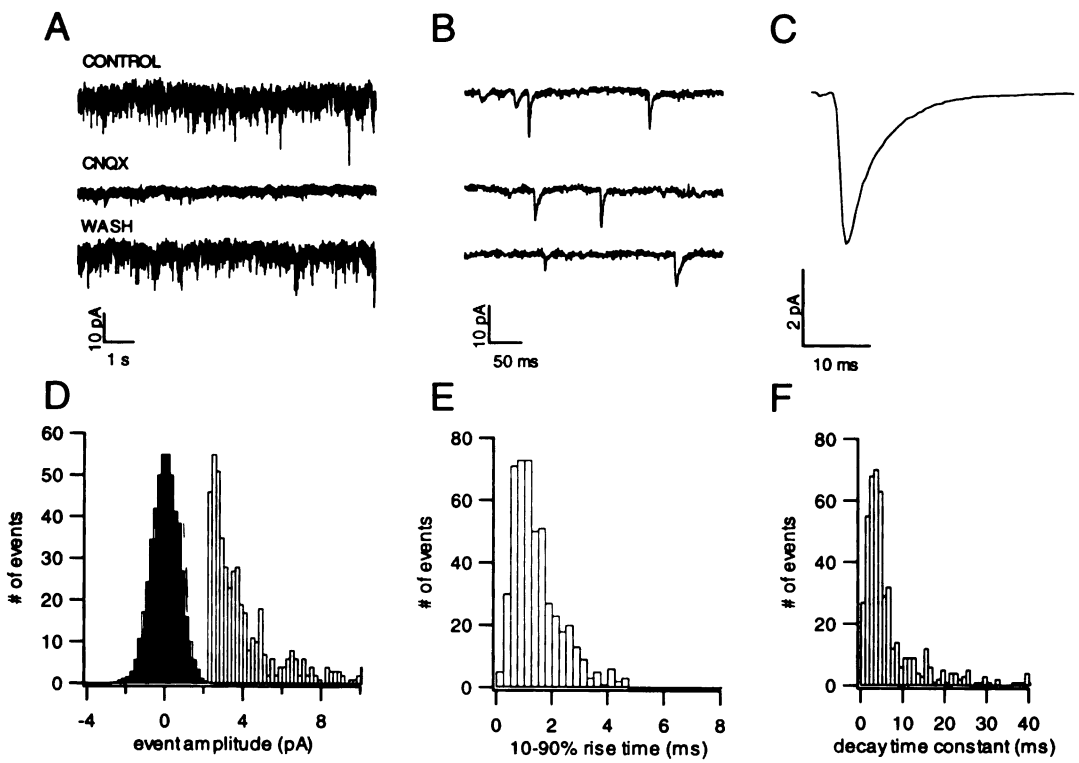
A
CONTROL
CNQX
WASH
10 pA
1 s
B
10 pA
50 ms
C
2 pA
10 ms
D
# of events
event amplitude (pA)
E
# of events
10-90% rise time (ms)
F
# of events
decay time constant (ms)

presence of only one kinetically distinguishable type of event. The mean 10-90% rise time of the average event from all the cells was 1.34 ± 0.25 ms (mean ± S.D., # cells = 49, # events = 43,885). The decay phase of the events was well described by a single-exponential curve. The mean decay time constant of the average event from all cells was 4.08 ± 1.03 ms (mean ± S.D., # cells = 49, # events = 43,885). These kinetic values are comparable to non-NMDA receptor-mediated events found in other neurons, in particular cells from the ganglion cell layer in salamander (Taylor et al., 1995; Matsui et al., 1998; Gao and Wu, 1999).

Non-NMDA glutamate receptors are comprised of two principal classes, namely AMPA and kainate receptors. To confirm the presence of AMPA receptors on amacrine cells, we examined the effect of the cyclothiazide (20 uM) on the amplitudes and decay time constants of the excitatory spontaneous events. Cyclothiazide preferentially inhibits the desensitization of AMPA-type receptors over kainate-type receptors (Partin et al., 1993; Wong and Mayer, 1993). Fig 1.4A shows a comparison of the average waveform in control versus in cyclothiazide from a single cell. Consistent with inhibition of AMPA receptor desensitization, cyclothiazide increased the amplitude from 4.1 pA to 6.1 pA (38% increase) and the decay time constant from 6.8 ms to 9.6 ms (40% increase). In Fig 1.4A, the average waveform in control was scaled to match amplitudes for better comparison of the decay phases. Fig 1.4B shows the cumulative distributions of the decay time constants in control and in

Fig 1.4: The desensitization blocker cyclothiazide prolongs the decay time of the fast excitatory events. The recording condition matched those described in Fig 1. A) Cyclothiazide (20 μM) in the external solution prolonged the decay time constant of the mean event waveform compare to control solution by 2.8 ms, or 40%. Since the mean waveform in cyclothiazide was 38% larger in amplitude, the control waveform was scaled in order to compare decay phases. B) Cyclothiazide (20 μM) in the external solution shifted the cumulative decay time constant distribution toward longer times compared to control solution.

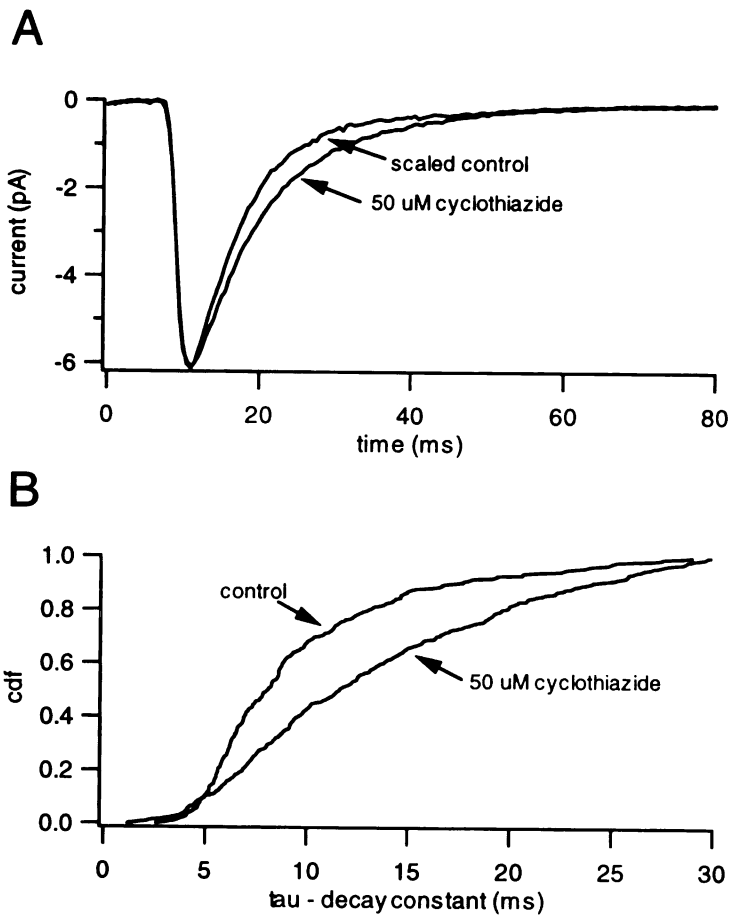

cyclothiazide. Clearly, cyclothiazide shifts the decay time constants toward longer times. These findings were consistent across all cells (n=3). Previous research showed that cyclothiazide prolongs and AMPA receptor antagonists block the evoked non-NMDA receptor-mediated responses in amacrine and ganglion cells, providing evidence for involvement of AMPA, rather than kainate, receptors (Lukasiewicz et al., 1997; Shen et al., 1999; Tran et al., 1999). Our results show the additional finding that desensitization of the receptors occurs even at the level of spontaneous release which involve much lower concentrations of glutamate for much shorter times than evoked responses. However, our results do not address the possibility of a subpopulation of kainate receptors on amacrine cells in salamander retina in addition to the AMPA receptors.

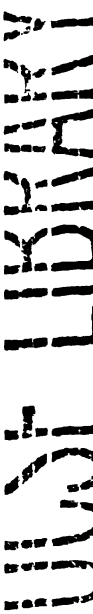

Amacrine cells possess mobile NMDA receptors with slow kinetics

We investigated whether NMDA-mediated spontaneous activity could be discerned in ON/OFF amacrine cells. Previous studies on light responses showed that both ON/OFF amacrine cells and ganglion cells possess NMDA receptors (Mittman et al., 1990; Dixon and Copenhagen, 1992). However, the evidence for NMDA-mediated spontaneous events has been inconsistent. In studies that examined the salamander retina, some studies found no NMDA spontaneous events in ganglion cells (Taylor et al., 1995; Matsui et al., 1998), while other findings documented NMDA events (Gao and Wu, 1999). NMDA-mediated events can be extremely slow during both the rising phase and the decay phase (Hestrin et al., 1990; Edmonds and Colquhoun, 1992; Edmonds et

al., 1995; Silver et al., 1996). This property makes these events more difficult to separate from the noise than the faster AMPA-mediated events because the background noise has more power at lower frequencies (See Chapter 4, Fig 4.2). This difficulty could explain the discrepancy in previous work.

Fig 1.5A shows recordings from an amacrine cell held at +50 mV in order to relieve the Mg^{2+} block on NMDA channels. Both recordings used strychnine (1 uM) and picrotoxin (200 uM) to block inhibitory events as well as CNQX to block non-NMDA receptors and cadmium (20uM) to isolate single quantal events. The bottom trace also included AP7, a specific NMDA receptor antagonist. Comparison of traces clearly shows that the spontaneous activity possessed an NMDA-mediated component. Fig 1.5B shows examples of the NMDA-mediated synaptic events while Fig 1.5C shows the average waveform of all events (n=229) detected from all cells (n=5). The calculated 10-90% rise time was 9.5 ms. Previous studies in other tissues have reported similar rise times for NMDA spontaneous synaptic events ranging from 8-20 ms (Hestrin et al., 1990; Edmonds and Colquhoun, 1992; Edmonds et al., 1995; Silver et al., 1996). These studies find that NMDA receptor-mediated events have a bi-exponential decay phase with a fast decay time constant ranging from 70-80 ms and a slow decay time constant ranging from 200 to 500 ms (Hestrin et al., 1990; Edmonds and Colquhoun, 1992; Edmonds et al., 1995; Silver et al., 1996). Our average waveform similarly had a fast decay time constant of 66.5 ms and a slow decay time constant of 312 ms. Fig 1.5D compares the amplitude distribution of detected events with the all-points histogram of a two-second event free

Fig 1.5: Kinetics of NMDA receptor-mediated spontaneous events. Spontaneous excitatory synaptic events were recorded from a voltage-clamped ON/OFF amacrine cell (Cs-methanesulfonate internal solution). The holding potential was +50 mV in order to relieve the Mg2+ blockage of the NMDA receptor channels. In order to isolate NMDA receptor-mediated events, the control solution contained CNQX, strychnine (STR), and picrotoxin (PTX) in order to block non-NMDA, glycine, and $GABA_A$ receptors, respectively. In addition, Cd^{2+} was used to isolate quantal events. A) The top trace shows the spontaneous activity of the amacrine cell held at +50 mV. The bottom trace shows that this activity was sensitive to the NMDA receptor antagonist AP7 (20 μM). B) Examples of the spontaneous synaptic events taken from the top trace in panel A. C) The mean event waveform averaged from all the events from all cells had a 10-90% rise time of 10 ms and a bi-exponential decay phase with a short time constant of 66.5 ms and a long time constant of 312 ms. D) The open bars show the amplitude distribution of the events from the top trace in panel A. The solid bars show the all points histogram of a two-second event free segment of the same trace scaled to match the peak of the event amplitude distribution shown by the open bars. The graph reveals that the background noise was very high at +50 mV; therefore, only events larger than 10 pA were selected. E) The bar graph of the 10-90% rise time distribution of all the events from all cells had a single mode of at approximately 10 ms.

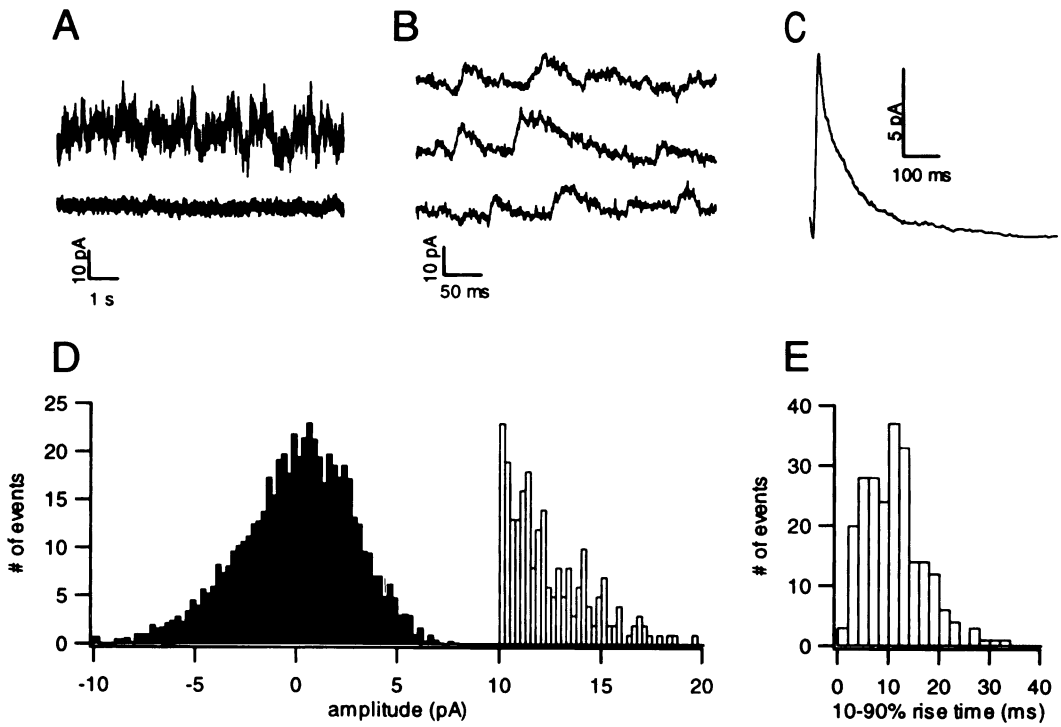
A
10 pA
1 s
B
10 pA
50 ms
C
5 pA
100 ms
D
# of events
25
20
15
10
5
0
-10
-5
0
5
10
15
20
amplitude (pA)
E
# of events
40
30
20
10
0
0
10
20
30
40
10-90% rise time (ms)

recording segment. The recordings at a holding potential of +50 mV consistently had higher noise levels than at –70 mV. The increased noise coupled with the higher difficulty in detection provided reason to select a higher amplitude threshold for detection of NMDA-mediated events. The events detected had a unimodal rise time distribution (Fig 1.5E), suggesting a single kinetic population. Since the variability in the decays phase of these events was very large, the decay time constant histograms did not yield informative distributions. Once, the clear kinetic distinction between non-NMDA and NMDA-mediated events was established, we examined the recordings that were done before we used CNQX to block the non-NMDA-mediated events. If non-NMDA and NMDA receptors were co-localized, evidence of spontaneous events that had the fast rising phase of the non-NMDA kinetics and the slow decay phase of the NMDA kinetics should have been evident as seen in other systems (Bekkers and Stevens, 1989), but such events were never observed (data not shown), suggesting that the two types of receptors do not co-localized in the bipolar-to-amacrine cell synapse.

Previous work has shown that central neurons in culture have extra-synaptic NMDA receptors which have the ability to migrate into the synapse (Tovar and Westbrook, 1999). As a final characterization of amacrine cell NMDA receptors, we investigated whether NMDA receptors are mobile in our more physiological preparation. While holding amacrine cells at -70 mV, we isolated NMDA receptor-mediated responses by perfusing a low Mg^{2+} external solution containing CNQX, PTX, and STR while stimulating with a 10 ms flash. Blockade

of inhibition also increased the light response to help ensure maximum glutamate release. By applying the activity-dependent NMDA receptor antagonist MK801 while stimulating with light , we were able to block those receptor activated by the light-evoked release while leaving any extra-synaptic receptors unaffected. The first panel in Fig 1.6A shows the overlap of NMDA-mediated light responses to a set of five light flashes of equal intensity separated by thirty seconds. The responses are all equal in amplitude indicating that the effects of light adaptation are not playing a significant role. The second panel is a repeat of the first after a three minute delay, showing that the light responses were robust and reproducible. As the third set of traces in Fig 1.6A shows, MK801 (10 μM) effectively blocks the flash response. Since MK801 is an irreversible blocker of the channel, even after MK801 is removed from the external bath, the response should still be inhibited. However, as shown by the fourth set of traces in Fig 1.6A, the response recovered after 3 minutes of wash. These finding are shown more clearly in a the bar graph of the normalized amplitudes of the responses shown in Fig 1.6B. The recovery from MK801 inhibition was found in all cells studied (# of cells = 5) as shown in Fig 1.7A. According to the model of mobile receptors, this recovery is due to the migration of functional extra-synaptic receptors into the synaptic cleft. This model is supported by the experiment perfusing both MK801 and NMDA during the light flash. As shown in Fig 1.7B, under these conditions, the light response did not recover after wash (# of cells = 4). Presumably, the NMDA activates the extra-synaptic receptors so that they are blocked by MK801 and cannot restore synaptic function after they migrate

Fig 1.6: NMDA responses recover from inhibition by the activity-dependent blocker MK801. The current responses of ON/OFF amacrine cells to 10 ms flashes of light were recorded in a low Mg2+ (0.5 mM) external solution containing CNQX to block non-NMDA receptors, strychnine to block glycine receptors, and picrotoxin to block $GABA_A$ and $GABA_C$ receptors. A) The first set of traces shows the responses to a series of five 10 ms light flashes were given 30 seconds apart. After 3 minutes, the flash series was presented again with no change in the response amplitude as shown in the second set of traces. After 3 minutes, MK801 (10 μM) was added to the external medium and a third flash series was started. As shown by the third set of traces, the flash response was almost completely inhibited. Due to dead space in the perfusion system, inhibition was usually not achieved until the third flash. Once inhibition was achieved, MK801 washout was begun. After 3 more minutes of wash, a fourth series of flashes was presented. As shown in the last set of traces, the response to the first flash showed almost full recovery from inhibition. The subsequent responses were all inhibited probably due to the difficulty in washing out the MK801. B) The bar graph shows the amplitudes of the responses shown in panel A.

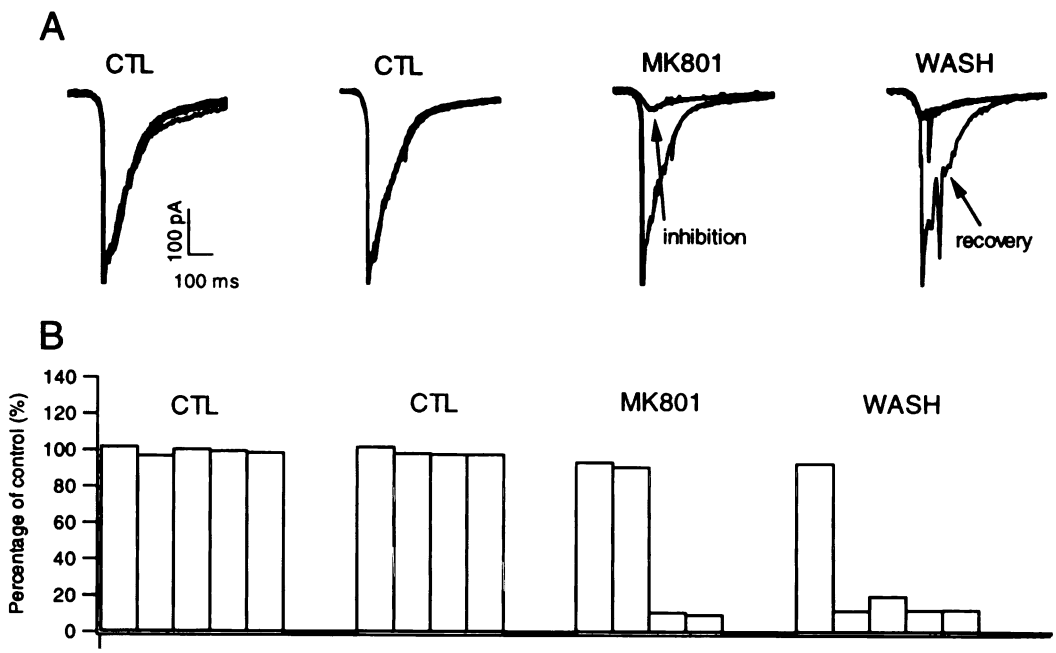

Fig 1.7: Extrasynaptic NMDA receptors can migrate into the synapse. The recording conditions and the flash protocol were the same as described in Fig 4 A) The results from all cells in the study (# of cells = 5) showing that the flash responses were inhibited by MK801 and then recovered after washout. According to our model, MK801 only can block NMDA receptor gated channels that were activated by the light response, leaving extrasynaptic receptors unaffected. The recovery, then, resulted from extrasynaptic receptors migrating into the synapse to restore function. B) The results from all cells (# of cells = 4) showing that the recovery from inhibition was inhibited by perfusion with NMDA and MK801 simultaneously. According to the model, since the NMDA activates extrasynaptic NMDA receptor gated channels so that they can be blocked by MK801, functional receptors remain to migrate into the cleft to restore synaptic function. C) A control experiment showing in the same cell that while NMDA alone did not block recovery of the flash response, NMDA with MK801 did inhibit the recovery.

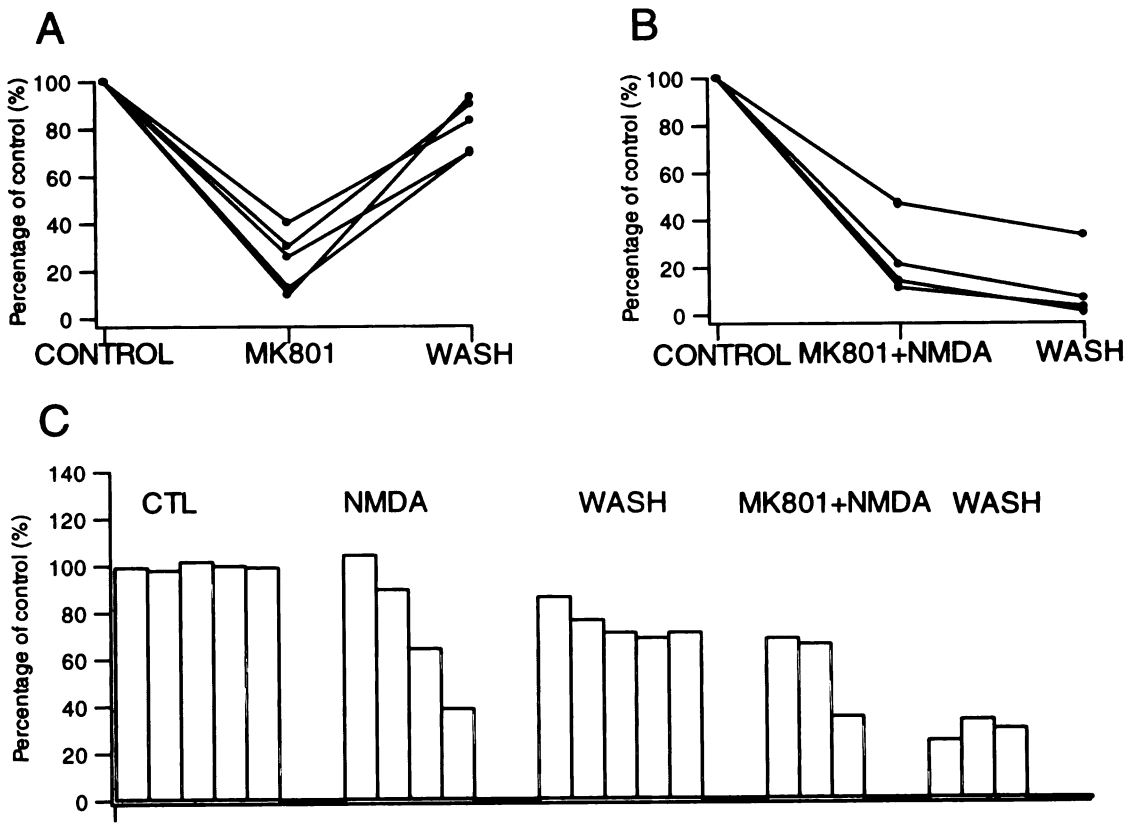
A
Percentage of control (%)
100
80
60
40
20
0
CONTROL
MK801
WASH
B
Percentage of control (%)
100
80
60
40
20
0
CONTROL
MK801+NMDA
WASH
C
Percentage of control (%)
140
120
100
80
60
40
20
0
CTL
NMDA
WASH
MK801+NMDA
WASH

into the cleft. To ensure that the inhibition of recovery was not to due to non-specific effects of NMDA, we also perfused NMDA without MK801 and found that NMDA alone does not block the recovery of the light response. The results from one cell are shown in the bar graph in Fig 1.7C.

Electrotonic filtering distorts the receptor kinetics only marginally

To investigate whether electrotonic filtering by dendrites played a large role in determining the kinetics of the spontaneous events, we compared the rise time with the amplitude and decay time constant of the events in each cell to see if they were correlated (Rall, 1969). Fig 1.8A and B show examples of plots of decay time constants (Fig 1.8A) and amplitudes (Fig 1.8B) versus rise times for detected glycinergic events from an amacrine cell. As with this example, no significant correlation was found in any of the cells included in this study (# cells = 17), providing evidence that the kinetics of the events were not determined primarily by dendritic filtering. Fig 1.8C and D show the corresponding correlation graphs for GABAergic events from an amacrine cell. Similarly, no correlations were found for any of the cells included in this study (# cell = 25)

Since AMPA receptor-mediated events have faster kinetics than the inhibitory events, evidence of distortion by filtering should be more obvious when examining these events. However, when the different parameters were correlated for AMPA receptor-mediated events from an amacrine cell (Fig 1.9A and B), no significant correlation was discovered. This result was found in all cells (# cells = 49), indicating that filtering did not play a major role in determining the observed kinetics of the events. However, when the rise times and decay

Fig 1.8: Electrotonic filtering did not significantly affect the observed kinetics of inhibitory spontaneous events. A) For all the glycinergic events in a single recording, the decay time constants were plotted against the 10-90% rise times. No correlation was found. B) For all the glycinergic events in a single recording, the event amplitudes were plotted against the 10-90% rise times. No correlation was found. C) For all the GABAergic events in a single recording, the decay time constants were plotted against the 10-90% rise times. No correlation was found. D) For all the GABAergic events in a single recording, the event amplitudes were plotted against the 10-90% rise times. No correlation was found.

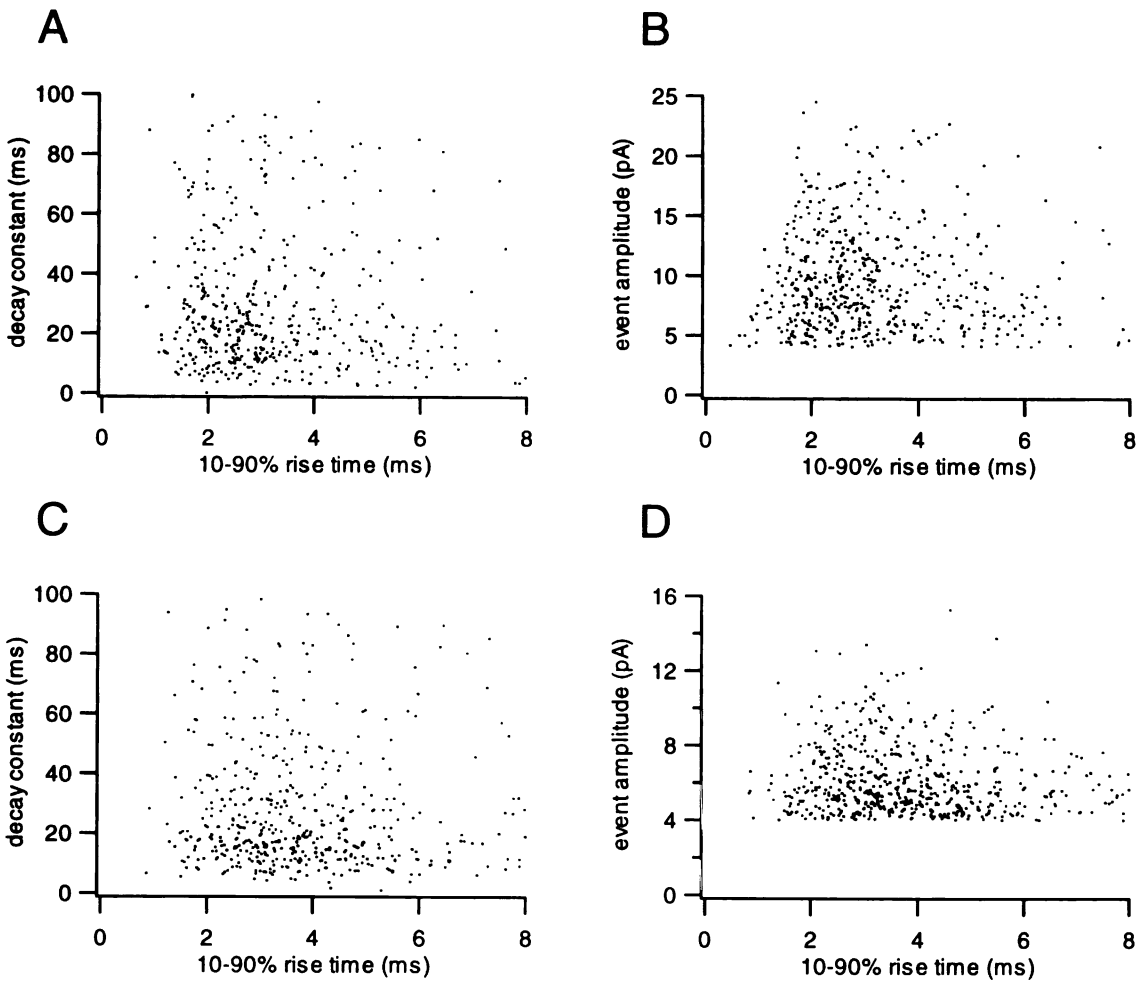

Fig 1.9: Electrotonic filtering did not significantly affect the observed kinetics of AMPA receptor-mediated events. A) For all the events in a single recording, the decay time constants were plotted against the 10-90% rise times. No correlation was found. B) For all the events in a single recording, the event amplitudes were plotted against the 10-90% rise times. No correlation was found. C) For all the mean waveforms from all cells, the decay time constants were plotted against the 10-90% rise times. A linear fit of the points resulted in a correlation coefficient of 0.58, showing that events with longer rise times tended to have longer decay time constants. This suggests that differences in space clamp from cell to cell may have slightly affected the observed kinetic values.

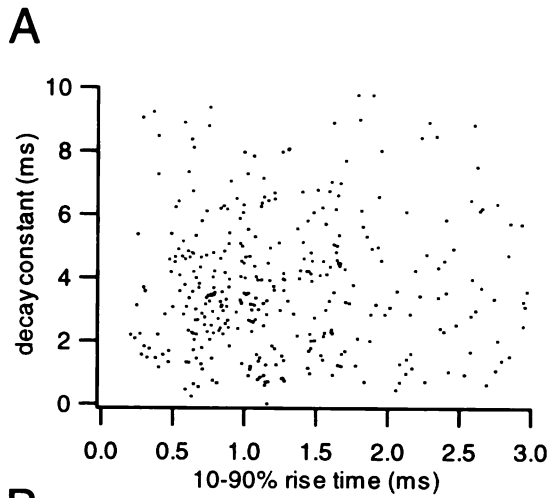

time constants of the average events of the cells were compared, a slight correlation was found. Fig 1.9C shows a graph of decay time constants versus time constants. However, as the graph shows, the effect of the correlation would only cause a slight overestimation in the kinetics of the AMPA events.

rise times from the average AMPA waveform from all cells (# cells = 49) along with a linear regression line of the data. The average waveforms with longer rise times had a small tendency to have longer decay time constants (R2=0.58). This effect most likely results from varying degrees of space clamp during the recordings from different cells. Cells that were less well space-clamped would tend to have events with slower kinetics, increasing both rise times and decay

Discussion

This study showed that the ON/OFF amacrine cells in the neotenous salamander retina exhibited spontaneous synaptic activity mediated by glutamate, glycine, and GABA. Glutamate-mediated spontaneous activity had separate NMDA and non-NMDA components. The non-NMDA events sensitive to CNQX had relatively fast kinetics with a mean 10-90% rise time of 1.34 ms and a mean decay time constant of 4.08 ms. The NMDA events sensitive to AP7 were much slower with a calculated rise time of 9.5 ms and biexponential decay phase with a fast time constant of 66.6 ms and a slow decay time constant of 312 ms. Similar to other studies in retinal ganglion cells, sEPSCs with dual-component decay phases were not observed (Taylor et al., 1995; Matsui et al., 1998), suggesting that sEPSCS with both non-NMDA and NMDA components did not occur. The inhibitory neurotransmitters glycine and GABA mediated spontaneous events that were very similar in kinetics to each other. The glycine events had a mean rise time of 2.71 ms and a decay time constant of 20.68 ms, while the GABA events had a mean rise time of 2.96 ms and a decay time constant of 22.67 ms

The kinetics of AMPA receptor-mediated events are similar in amacrine and ganglion cells

Recent findings have shown that the synaptic transmission from a given presynaptic cell to two different postsynaptic cells can have very different properties. Similarly, in the retina, Dixon and Copenhagen (1992) showed that bipolar cell transmission to transient amacrine cells differs from transmission to

sustained amacrine cells because transient amacrine cells use both NMDA receptors and non-NMDA receptors to mediate synaptic input, while sustained cells, are exclusively driven by non-NMDA receptors. In this manner, different postsynaptic cells can interpret the same neurotransmitter release differently. Because ganglion cells serve as the final output neurons of the retina while amacrine cells serve as interneurons, there is no a priori reason to assume that synaptic transmission to these two types of cells has to be the same. However, the kinetics of the AMPA events found in amacrine cells were comparable to those found in ganglion cells . This finding supports the idea that at the level of the quantal response at least, the AMPA-mediated glutamatergic synaptic transmission from bipolar to amacrine cell is very similar to transmission from bipolar to ganglion cells.

The kinetics of inhibitory events differ in amacrine and ganglion cells

In rat ganglion cells, the mono-exponential decay of $GABA_A$ receptor-mediated events was faster than the decay of glycine-mediated events . However, our results show no significant difference between the two types of inhibitory events in salamander amacrine cells. This finding is similar to the case reported in mouse ganglion cells . These differences in kinetics between the glycine-mediated events in rat versus mouse and salamander may reflect species-selective expression of isoforms of the receptors.

A previous study on cells from the ganglion cell layer described the kinetics of the inhibitory spontaneous events using a bi-exponential curve . Our analysis found that only 20 to 25% of the inhibitory events were significantly fit

better with a bi-exponential curve. Visual inspection of these events confirmed that they appeared to have a bi-exponential decay. The bi-exponential glycine events had average decay time constants of 2.64 ms and 28.50 ms, while bi-exponential GABA events had average decay time constants of 3.05 and 48.49 ms. These values do not match the previous values measured in tiger salamander ganglion cells, which were 12.4 and 241.2 ms for glycine events and 10.49 ms and 89.51 ms for GABA events . However, the differences may result from the method of event detection and characterization. Having spontaneous events that have a bi-exponential decay may indicate that the released neurotransmitter is activating two subtypes of the receptor that have different kinetics. Alternatively, the gating of the channels could be such that it produces a biphasic decay as is seen for NMDA receptor-gated channels (Hestrin et al., 1990).

Amacrine cell glutamatergic input activates mobile NMDA receptors

Some previous reports did not find NMDA-mediated spontaneous events in neurons of the ganglion cell layer (Taylor et al., 1995; Matsui et al., 1998). In contrast, Gao and Wu (1999) published results showing an NMDA component to the spontaneous activity in the same cells. NMDA-mediated events can be extremely slow during both the rising phase (up to 20 ms) and the decay phase (fifty to hundreds of milliseconds) (Hestrin et al., 1990; Lester et al., 1990; Edmonds and Colquhoun, 1992; Edmonds et al., 1995; Silver et al., 1996). This property makes these events more difficult to separate from the noise than the faster AMPA-mediated events, which could explain the discrepancy in previous

work. Our finding of NMDA-mediated spontaneous activity in amacrine cells matched the finding in ganglion cells by Gao and Wu (1999).

A previous study on cultured hippocampal neurons used the presence of spontaneous events with both a fast non-NMDA component and a slow NMDA component as evidence that the two types of receptors were co-localized (Bekkers and Stevens, 1989). In contrast, our findings from tiger salamander amacrine cells show that individual spontaneous events recorded +50 mV without excitatory neurotransmitter antagonists did not have a dual component decay phase. The fast non-NMDA events appeared independently of the slow NMDA events, suggesting that NMDA and non-NMDA receptors may not be co-localized at the amacrine cell input synapses in tiger salamander. Even more, it suggests that perhaps glutamatergic synapses are either mediated postsynaptically by either NMDA or AMPA but not both.

In support of previous work in culture (Tovar and Westbrook, 1999), the NMDA receptors on transient amacrine cells seem to be mobile. The receptors may be continuously moving in and out of the synaptic cleft. Dynamic systems tend to be useful for their adaptive properties. In this case, the amacrine cell could use the mobility of the receptors to modulate synaptic transmittion by having receptors migrate into the cleft to increase synaptic strength. In addition, having the reserve NMDA receptors already on the plasma membrane is much more efficient then transporting new receptors to the membrane when the need arises. Systems that use plasma membrane mobility have not been documented with receptor types other than NMDA receptors. However, a different version of

dynamic receptor control has been described with AMPA receptors in which the number of functional AMPA receptors is controlled by endocytosing varying number of receptors into cytoplasmic vesicles in order to modulate synaptic strength (Turrigiano et al., 1998; Man et al., 2000; Turrigiano, 2000). Perhaps, dynamic receptor control is a common theme in synaptic transmission, which has been implement in multiple ways. Alternatively, perhaps NMDA receptors simply lacked an evolutionary drive to have an anchoring mechanism to restrict them to the synaptic cleft.

Chapter 2

Characterization of neurotransmitter release from amacrine and bipolar cells

Introduction

Often, spontaneous activity can be recorded as a mixture of single quantal miniature events and larger amplitude multi-quantal events. At synapses with a spiking presynaptic neuron, sodium action potentials cause a relatively large depolarization that can initiate multi-quantal release by the virtually simultaneous activation of multiple release sites. However, synaptic transmission to amacrine cells is different because the presynaptic bipolar and amacrine cells do not rely on sodium action potentials for signaling. Bipolar cells do not even possess fast-activating sodium channels, and although amacrine cells do exhibit sodium spikes, those spikes are not required for synaptic transmission . In many neural systems comprised exclusively of spiking neurons, such as hippocampus, blocking sodium spikes ensures that recorded spontaneous postsynaptic events will consist of only single quantum. It is an open question whether action potential-mediated multi-quantal release can be observed in amacrine cells. In fact, evidence shows that amacrine cells still produce unexpectedly large events in presence of tetrodotoxin, a sodium channel blocker . These large events may result from a variation in the amount of transmitter released for each quantum (Frerking et al., 1995). However, a hypothesis that remains unexplored proposes that calcium-driven action potentials could elicit multi-quantal release to produce those large events. Evidence has shown that bipolar cells undergo such calcium

action potentials (Burrone and Lagnado, 1997; Zenisek and Matthews, 1998; Protti et al., 2000), and these calcium spikes may also exist in amacrine cells since they, like bipolar cells, use L-type calcium channels to trigger synaptic release (Bieda and Copenhagen, 2000).

Once all sodium and calcium-dependent neurotransmitter release has been blocked, we assume that the remaining spontaneous activity represents postsynaptic miniature responses from quantal release. Characterization of the miniature events quantifies the basic unit of synaptic transmission. This data serves as the foundation for further studies of synaptic transmission to amacrine cells. Here, applying deconvolution methods, we use the quantal waveform characterization to derive the neurotransmitter release function of amacrine and bipolar cells during a step of light. These functions provide information about the number and timing of quantal events during light stimulation.

The release function of bipolar cells has particular significance because one of the fundamental properties of bipolar cells is the use of synaptic ribbons to tether neurotransmitter vesicles near the release sites. This synaptic ribbon is a highly specialized synaptic structure not found in many other types of neurons. Possibly, the presence of this ribbon is related to neurons that release transmitter in a more continuous fashion rather than phasic. The ribbon may serve to facilitate the transfer of vesicles to the active release sites in order to maintain continuous release. The vesicles in the terminal have been divided into essentially four different functional pools (von Gersdorff and Matthews, 1994; von Gersdorff et al., 1996; von Gersdorff and Matthews, 1997). The first pool is the

immediately releasable vesicles which represents the vesicles that are docked at the release sites and ready to be released. The second involves the vesicles tethered to the ribbons that can be transferred to the release sites after the sites have been emptied with a time constant on the order of 10 ms. The third involves the vesicles immediately above each ribbon which has been named the fast reserve pool. This pool seems to have enough vesicles to replenish the ribbons once and can do so with an exponential time constant of approximately 8 s (> 20 s for complete refilling). The final pool involves the large reservoir of vesicles in the center of the terminal that presumably refills the fast reserve pool. In these studies of the different vesicle pools, isolated bipolar cells were patch-clamped and depolarized to levels intended to mimic light-responses while capacitance measurements were used to monitor the exocytosis and endocytosis of vesicles. After one depolarization stimulus, a second depolarization induced a much attenuated increase in capacitance, which the authors attributed to the depletion of vesicles from the synaptic ribbon. If the two stimuli were separated by at least 20 s, then the second response was comparable to the first, presumably because the ribbon had enough time to completely refill (von Gersdorff and Matthews, 1994; von Gersdorff et al., 1996; von Gersdorff and Matthews, 1997).

The question remains whether this depletion effect is seen in a more physiological preparation using actual light stimulation. We approach this question both theoretically and experimentally. First, we derive the quantal release function for bipolar cells during maximal response light stimulation. By

comparing the number of quanta released during a maximum response with the anatomical numbers of vesicles and synaptic ribbons quantified in previous studies, we can evaluate the likelihood that the terminals could be depleted by light stimulation. Second, to examine the question experimentally, we used paired light flashes at an intensity that caused maximum light responses in amacrine cells to see if the second flash showed signs of attenuation due to depletion.

Results

Amacrine cell multi-quantal release results from activation of both calcium channels and voltage-gated sodium channels

The dependence of neurotransmitter release on sodium spiking was examined by using the sodium channel blocker tetrodotoxin (TTX) and the dependence on voltage-gated calcium channels was examined using Cd^{2+}. Fig 2.1A and B show the effect of TTX and TTX with cadmium on the cumulative amplitude distribution (left graphs) and average event waveforms (right graphs) of glycine and of $GABA_A$ receptor-mediated events, respectively. The recordings were done at +10 mV with SR95535 to isolate glycine events and strychnine to isolate GABAergic events. TTX significantly shifted the amplitude distributions of glycinergic and GABAergic events towards smaller events by removing the larger events compared to control (Fig 2.1A and B, left graphs). In addition, the average amplitude of the average event waveform was reduced (Fig 2.1A and B, right graphs). This suggests that the larger amplitude inhibitory events resulted from sodium spike dependent multi-quantal release from presynaptic amacrine cells. Adding cadmium as well as TTX, then, shifted the amplitude distributions even farther towards smaller events by removing some of the larger events (Fig 2.1A and B, left graphs), suggesting that amacrine cells also possess calcium-dependent multi-quantal presynaptic release mechanisms. This effect was also shown as a reduction of the amplitude of the average event waveform (Fig 2.1A and B, right graphs). According to the KS test, TTX significantly shifted glycinergic amplitude distributions in 3 of 4 cells, and cadmium had an additional

Fig 2.1: Inhibitory multi-quantal release depends on both sodium and calcium channels. Inhibitory events were recorded from amacrine cells at a holding potential of +10 mV, the effective reversal potential of excitatory synaptic currents. A) The $GABA_A$ receptor antagonist SR95535 (10 uM) was used to isolate glycinergic synaptic events. The left graph shows an example of an amacrine cell where TTX (1 μM) shifted the cumulative amplitude distribution to toward smaller events and TTX (1 μM) plus Cd^{2+} (20 μM) shifted the distribution even further. The right graph shows that the amplitude of the average event waveforms for the same cell decreased with TTX and deceased even further with TTX plus Cd^{2+}. B) The glycine receptor antagonist strychnine (1 μM) was used to isolate GABAergic synaptic events. The left graph shows an example of an amacrine cell where TTX shifted the cumulative amplitude distribution to toward smaller events and TTX plus Cd^{2+} shifted the distribution even further. However, this effect is much weaker for GABAergic events than for glycinergic events. The right graph shows that the amplitude of the average event waveforms for the same cell decreased with TTX and deceased even further with TTX plus Cd^{2+}.

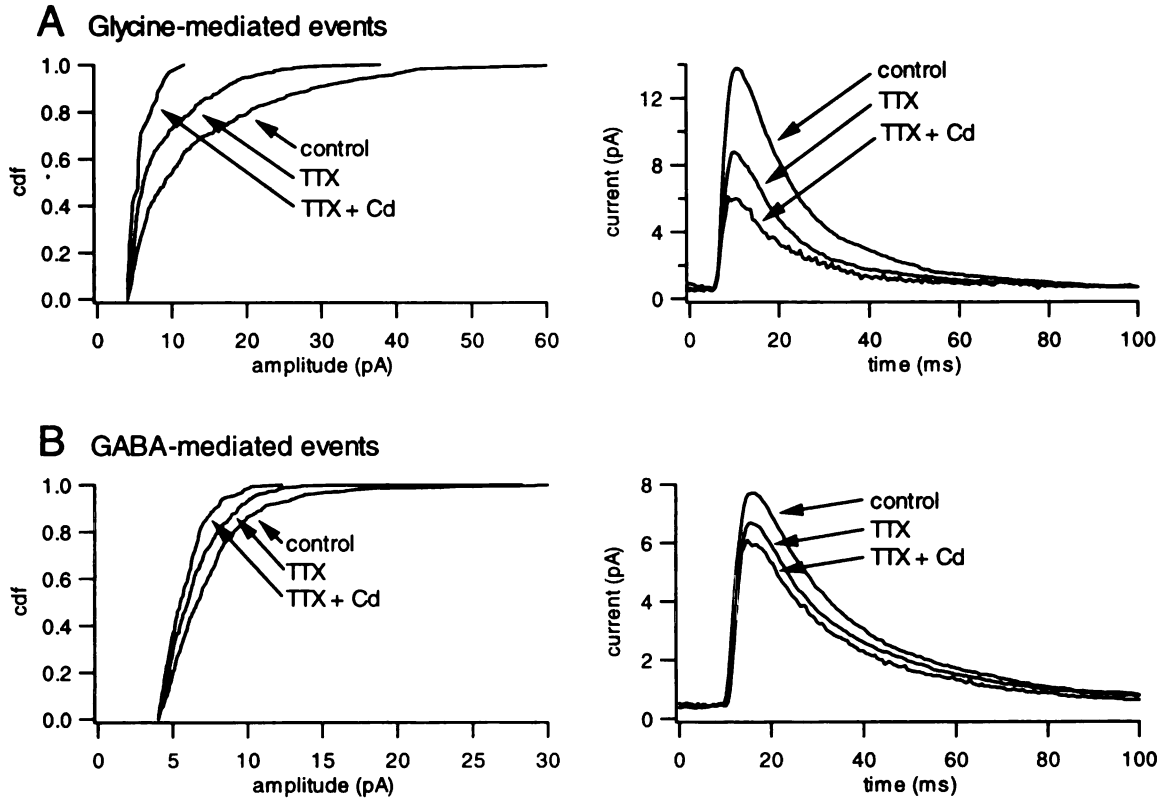
A Glycine-mediated events
cdf
1.0
0.8
0.6
0.4
0.2
0.0
0
10
20
30
40
50
60
amplitude (pA)
control
TTX
TTX + Cd
current (pA)
12
8
4
0
0
20
40
60
80
100
time (ms)
control
TTX
TTX + Cd
B GABA-mediated events
cdf
1.0
0.8
0.6
0.4
0.2
0.0
0
5
10
15
20
25
30
amplitude (pA)
control
TTX
TTX + Cd
current (pA)
8
6
4
2
0
0
20
40
60
80
100
time (ms)
control
TTX
TTX + Cd

effect in 2 of 3 cells (p=0.01). As for GABAergic amplitude distributions, TTX had a significant effect in 6 of 6 cells, and cadmium had an additional effect in 4 of 6 cells (p=0.01). These findings support the idea that both calcium and sodium-mediated activity contributes to neurotransmitter release from both glycinergic and GABAergic amacrine cells. However, as revealed by comparing Fig 2.1A with Fig 2.1B, the effects of both TTX and Cd^{2+} were much stronger for glycinergic amacrine cells. This suggests that voltage-activated sodium and calcium channels play a more pronounced role in glycinergic amacrine-to-amacrine synapses than GABAergic synapses.

Bipolar cell multi-quantal release results from activation of calcium channels but not sodium channels

Bipolar cells release as represented by the excitatory spontaneous activity recorded from amacrine cells was analyzed in a similar fashion using TTX and Cd^{2+}. Fig 2.2A shows examples of the cumulative amplitude distributions (left graph) and average waveforms (right graph) from events recorded at –70 mV in control, TTX (1 μM), and TTX plus Cd^{2+}(20 μM). Clearly, TTX had no effect on either the amplitude distribution or the average event (Fig 2.2A, left graph). The Kolmogorov-Smirnov test was used to determine if these distributions were significantly different statistically. TTX had no effect on the amplitude distributions in 5 of 6 cells (p=0.01). Supporting this result, TTX had no effect on the amplitude of the average event waveforms either (Fig 2.2A and B, right graph). This finding is consistent with the absence of voltage-activated sodium

Fig 2.2: Bipolar cell multi-quantal release depends on calcium not sodium channels. Excitatory events were recorded from amacrine cells at a holding potential of -70 mV, the effective reversal potential of inhibitory synaptic currents. A) The left graph shows an example of an amacrine cell where TTX (1 μM) had no effect but TTX (1 μM) plus Cd^{2+} (20 μM) shifted the cumulative amplitude distribution of synaptic events toward smaller events while TTX had no effect. The right graph shows how the amplitude of the average waveform in control conditions was unaffect by TTX alone but decreased by TTX plus Cd^{2+}. B) The two graphs show an example of an amacrine cell where neither TTX nor TTX plus Cd^{2+} had any affect on either the cumulative amplitude distribution or the averaged event waveform.

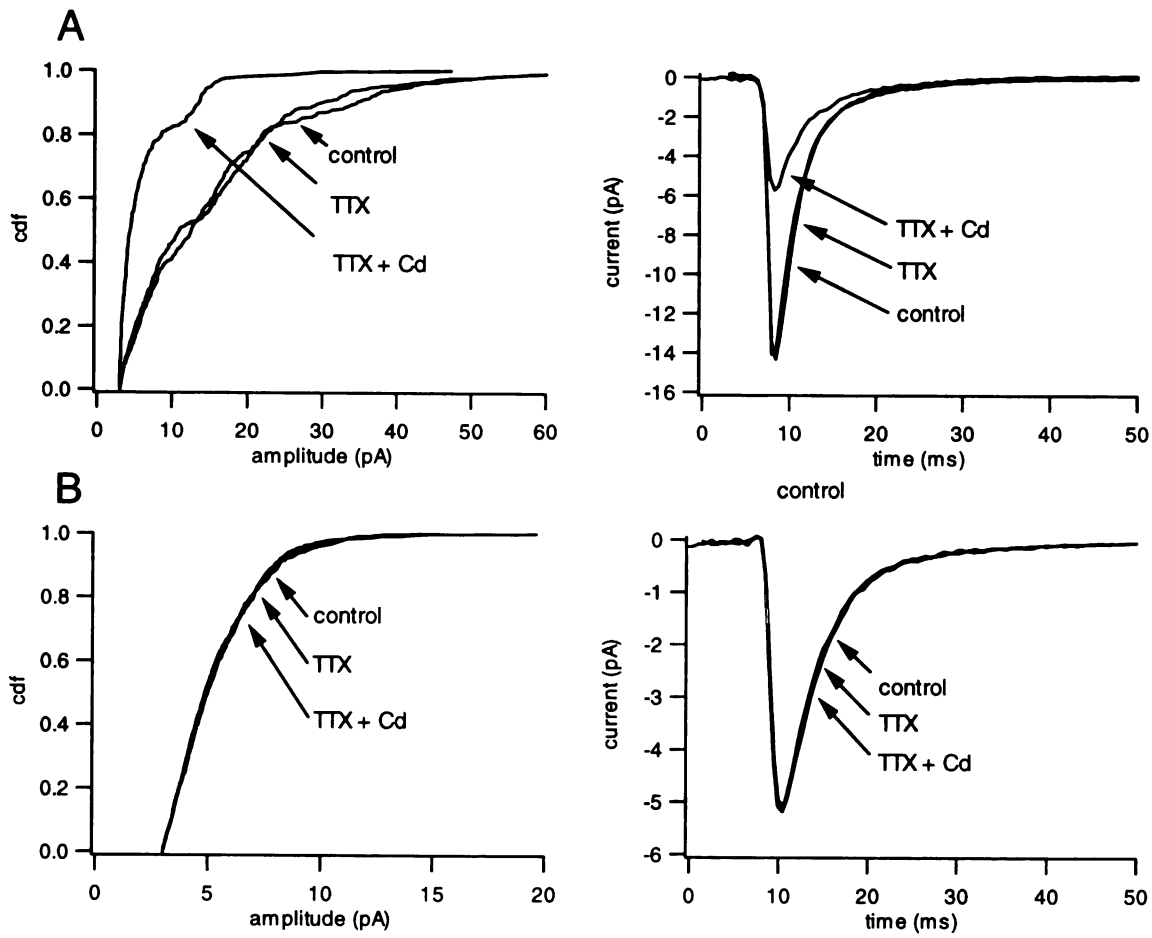
A
1.0
0.8
0.6
0.4
0.2
0.0
cdf
0
10
20
30
40
50
60
amplitude (pA)
control
TTX
TTX + Cd
0
-2
-4
-6
-8
-10
-12
-14
-16
current (pA)
TTX + Cd
TTX
control
0
10
20
30
40
50
time (ms)
B
1.0
0.8
0.6
0.4
0.2
0.0
cdf
0
5
10
15
20
amplitude (pA)
control
TTX
TTX + Cd
control
0
-1
-2
-3
-4
-5
-6
current (pA)
control
TTX
TTX + Cd
0
10
20
30
40
50
time (ms)

channels in bipolar cells. In contrast, the third curve in Fig 2.2A (left graph) shows that the amplitude distribution shifted towards smaller events in TTX and Cd^{2+} compared to TTX only, and Fig 2.2A (right graph) shows that the average event becomes much smaller. This effect is evidence that a calcium channel dependent process exists that causes multi-quantal release of transmitter. Calcium action potentials have been shown to exist in bipolar cells (Burrone and Lagnado, 1997; Zenisek and Matthews, 1998; Protti et al., 2000) and could theoretically underlie multi-quantal glutamate release. However, blocking voltage-gated calcium channels also causes smaller changes in membrane potential so that the shift toward smaller events may simply stem from smaller voltage changes independent of any type action potential. The KS test showed that a significant shift in the amplitude distribution in TTX plus Cd^{2+} compared to TTX only occurred in 2 of 4 cells ($p=0.01$). In the other two cells, neither TTX nor TTX plus Cd2+ had any effect on the event amplitudes. Fig 2.2B shows examples of the cumulative amplitude distributions (left graph) and average waveforms (right graph) from one such cell. Notably, these cells did not have large events even in control media, which suggests that not all bipolar cells have multi-quantal calcium-dependent exocytotic events. Interestingly, a study in goldfish showed that only a fraction of bipolar cells has light-evoked calcium-dependent spiking activity (Protti et al., 2000); therefore, if calcium action potentials do underlie the multi-quantal release from bipolar cells, our results are consistent with previous findings.

Quantal release underlying light-evoked currents

We sought to calculate the number of quanta released from presynaptic amacrine and bipolar cells that underlies typical light-evoked responses of amacrine cells and to approximate the timing of the release of these quanta. We assumed that the events recorded under conditions of TTX and Cd^{2+} were single quantal events; therefore, we used the average waveform calculated under these conditions to represent an average quantal response for a given amacrine cell. To estimate the number of quanta released during each light response, we divided the area under each light response by the area under the quantal waveform. To determine the quantal release function we used a computer program to deconvolve the observed response with the calculated quantal waveform by summating quantal responses until the result visually matched the observed light response recorded from the cell. Significantly, our deconvolution process assumed that only integer number of quanta could be released. These calculations do not take into account any possible effects of receptor desensitization.

To isolate inhibitory light responses, we recorded the current responses of amacrine cells at a holding potential of +10 mV, the effective reversal of the excitatory currents. Glycine-mediated light responses were recorded in the presence of the $GABA_A$ receptor preferring antagonist, SR95535 (10 uM), while GABA-mediated light responses were recorded in the presence of the glycine receptor preferring antagonist, strychnine (1 μM). Fig 2.3 shows an example of the glycine-mediated ON (top panel) and OFF (bottom panel) responses from an

Fig 2.3: Light-evoked quantal release function for glycine. Glycine receptor-mediated currents were isolated by using SR95535 (10 μM) to block GABA receptors and by holding the cells at the effective reversal potential for excitatory currents (+10 mV). A single two-second step of light was used to elicit the light response as shown by the line at the top of each panel. The top panel shows the ON response of an amacrine cell to a two second step of light (lower trace) as well as the reconstructed response (upper trace) derived from convolving the calculated quantal release function shown at the bottom of the panel with the calculated quantal event shown in the inset. The bottom panel shows the OFF response of an amacrine cell to a two second step of light (lower trace) as well as the reconstructed response (upper trace) derived from convolving the calculated quantal release function shown at the bottom of the panel with the calculated quantal event shown in the inset.

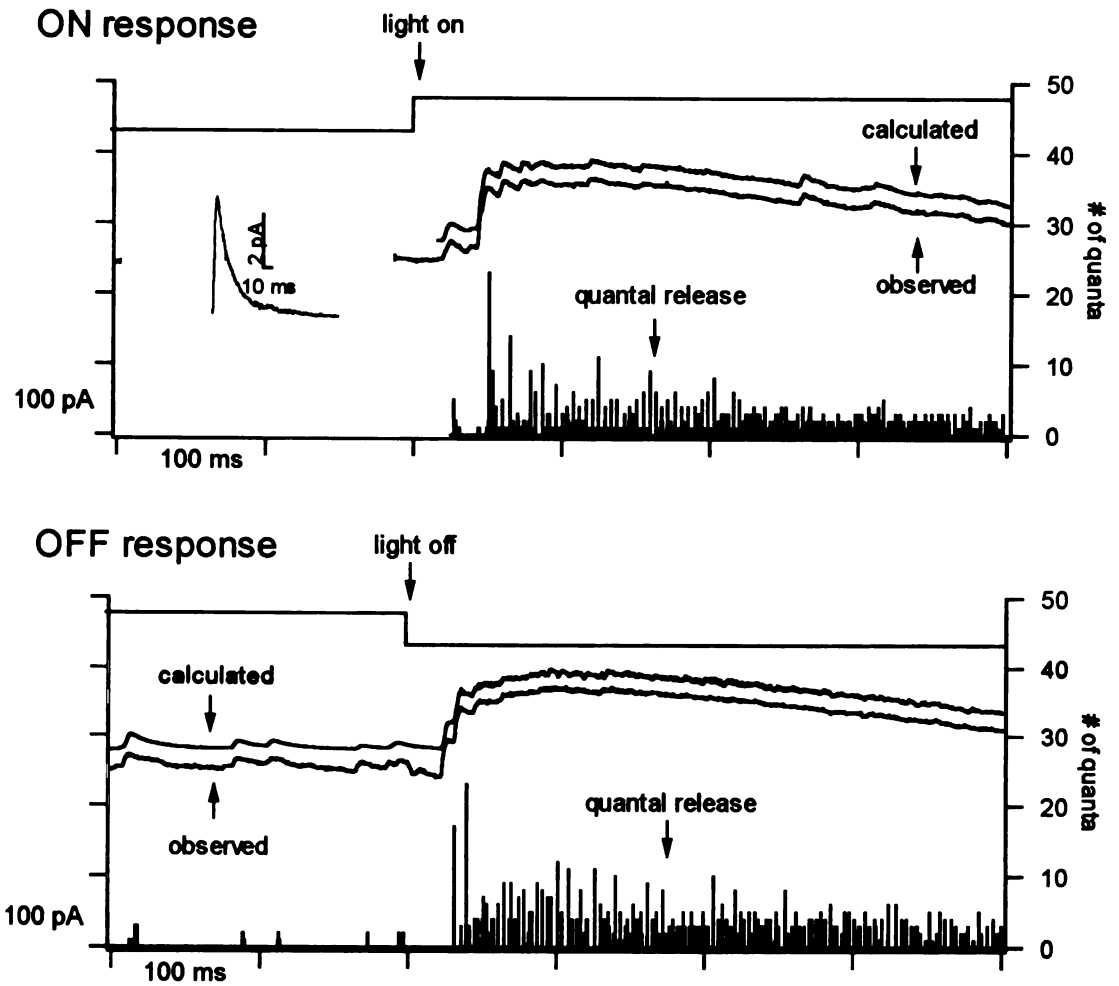
ON response
light on
calculated
observed
quantal release
2 pA
10 ms
100 pA
100 ms
# of quanta
50
40
30
20
10
0
OFF response
light off
calculated
observed
quantal release
100 pA
100 ms
# of quanta
50
40
30
20
10
0

amacrine cell when stimulated with a two second step of light (the lower of the two top traces in each panel). Fig 2.4 shows the same recordings in a different cell for GABA-mediated responses. The quantal waveforms used for the deconvolution for each cell is shown in the inset of the top panel. The quantal release functions resulting from the deconvolution process are shown at the bottom of each panel. Then, the calculated light responses derived by convolving the quantal event with the quantal release functions are shown (the higher of the two top traces in each panel) slightly offset from the recorded response to show that the observed and the calculated response match well. In a given cell, the ON and the OFF responses could be very different from each other, but across cells no great differences existed between the ON and OFF responses in terms of numbers of quanta. The numbers ranged from tens of quanta for small response to 1,000 quanta for the largest response recorded.

To isolate excitatory light responses, we recorded the current responses of amacrine cells at a holding potential of -70 mV, the effective reversal of the inhibitory currents. At this potential, the NMDA receptor-mediated currents are mostly blocked by the external Mg2+. Fig 2.5 shows an example of typical ON response (top graph) and OFF response (bottom graph) from an amacrine cell to a two second step of light with the calculated quantal event displayed in the inset of the top graph. The quantal release function resulting from the deconvolution process are shown at the bottom of each graph. As with the inhibitory light responses, the ON and OFF responses could vary in a given cell but were very similar when examined across cells.

Fig 2.4: Light-evoked quantal release function for GABA. GABA receptor-mediated currents were isolated by using strychnine (1 μM) to block glycine receptors and by holding the cells at the effective reversal potential for excitatory currents (+10 mV). A single two-second step of light was used to elicit the light response as shown by the line at the top of each panel. The top panel shows the ON response of an amacrine cell to a two second step of light (lower trace) as well as the reconstructed response (upper trace) derived from convolving the calculated quantal release function shown at the bottom of the panel with the calculated quantal event shown in the inset. The bottom panel shows the OFF response of an amacrine cell to a two second step of light (lower trace) as well as the reconstructed response (upper trace) derived from convolving the calculated quantal release function shown at the bottom of the panel with the calculated quantal event shown in the inset.

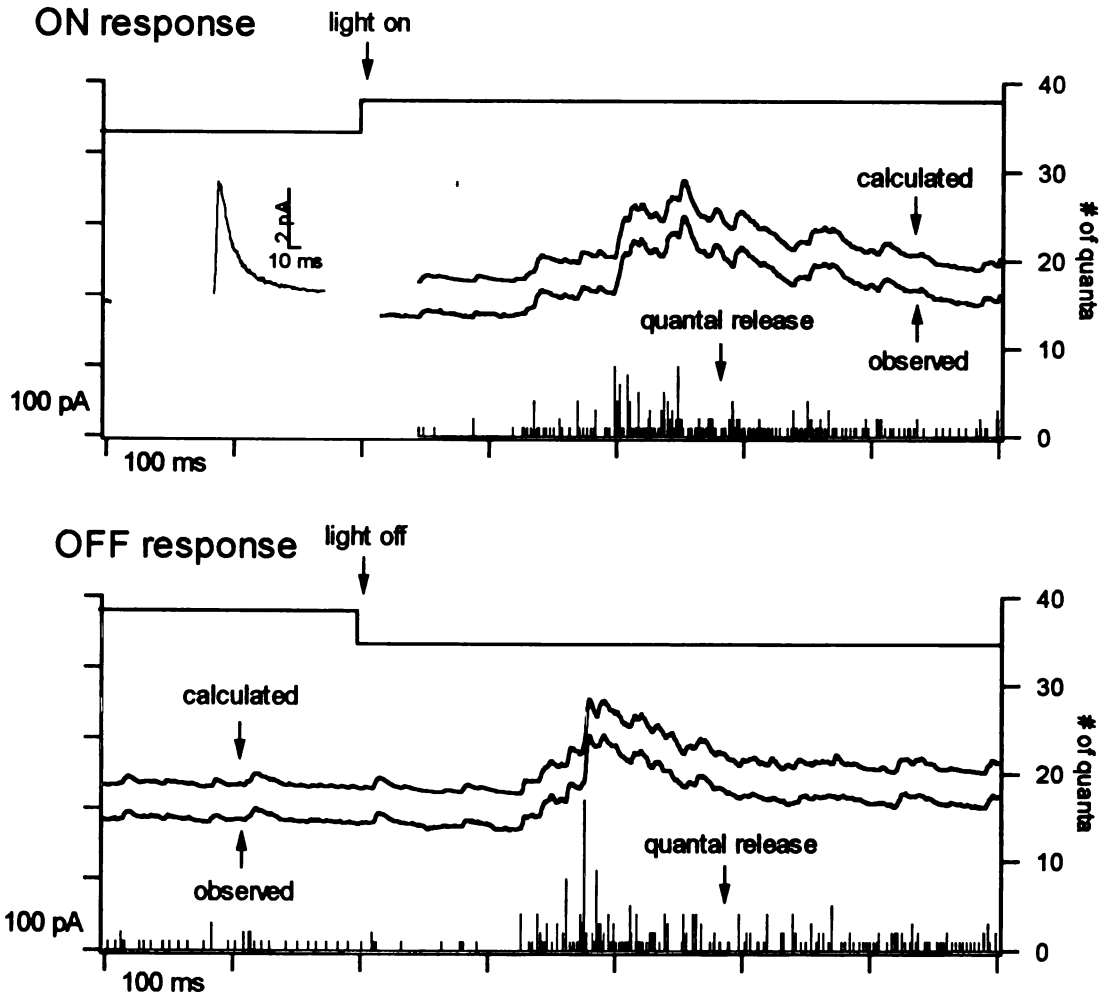
ON response
light on
40
30
20
10
0
# of quanta
calculated
2 pA
10 ms
quantal release
observed
100 pA
100 ms
OFF response
light off
40
30
20
10
0
# of quanta
calculated
observed
quantal release
100 pA
100 ms

Fig 2.5: Light-evoked quantal release function for glutamate. Glutamate receptor-mediated currents were isolated by holding the cells at the effective reversal potential for inhibitory currents (-70 mV). A single two-second step of light was used to elicit the light response shown by the line at the top of each panel. The top panel shows the ON response of an amacrine cell to a two second step of light (lower trace) as well as the reconstructed response (upper trace) derived from convolving the calculated quantal release function shown at the bottom of the panel with the calculated quantal event shown in the inset. The bottom panel shows the OFF response of an amacrine cell to a two second step of light (lower trace) as well as the reconstructed response (upper trace) derived from convolving the calculated quantal release function shown at the bottom of the panel with the calculated quantal event shown in the inset.

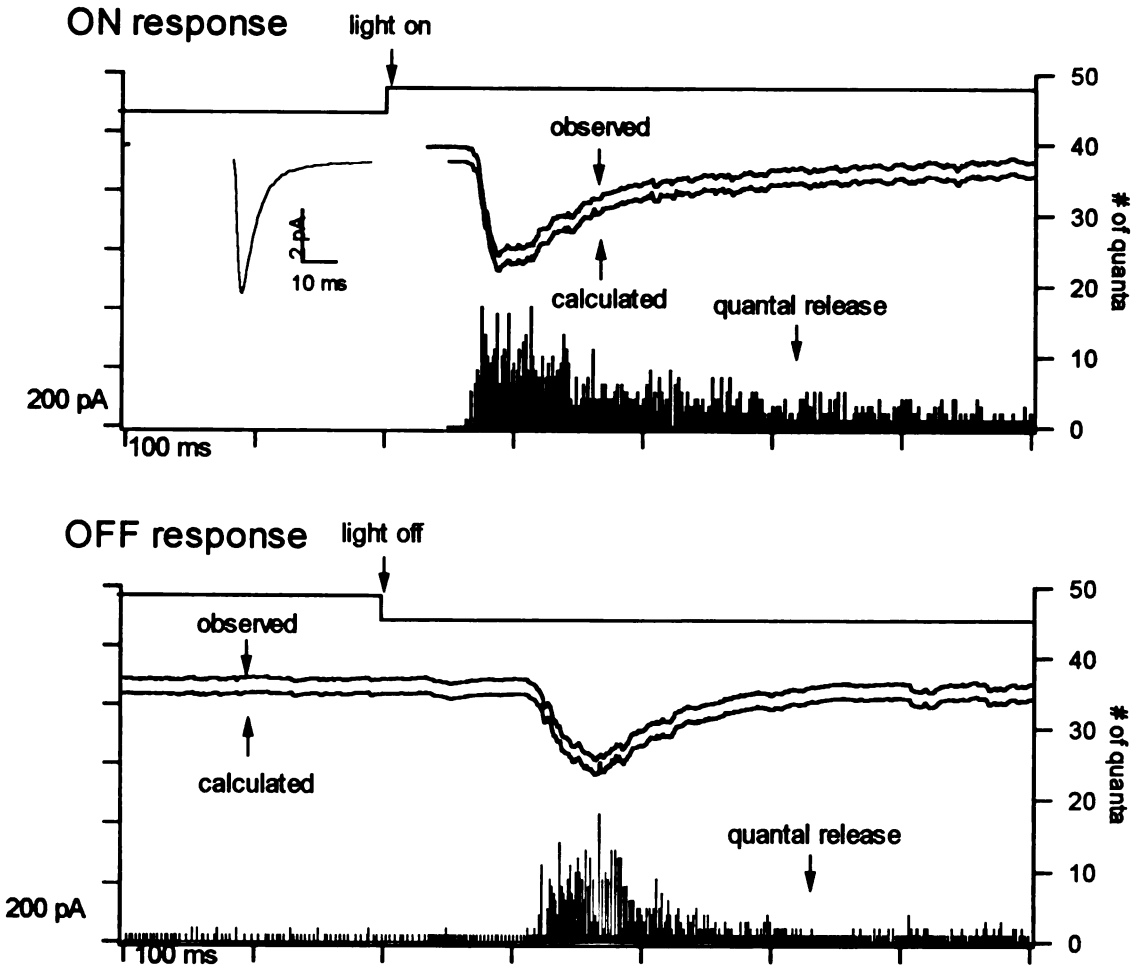
ON response
light on
observed
2 pA
10 ms
calculated
quantal release
200 pA
100 ms
50
40
30
20
10
0
# of quanta
OFF response
light off
observed
calculated
quantal release
200 pA
100 ms
50
40
30
20
10
0
# of quanta

For both excitatory and inhibitory light-evoked responses, the time course of release was largely asynchronous with the rise time lasting 30 to 50 ms, which is an order of magnitude slower than the rise time of even the slower inhibitory quantal events. At the time resolution of our recording (0.5 ms), the largest number of quanta release simultaneously was approximately 25 for glutamate, glycine, and GABA. Since glutamatergic events have much faster kinetics (approximately 1 ms 10-90% rise time and 4 ms decay time constant, See Chapter 1 Fig 1.3), the release function and the postsynaptic current response tended to follow each other very closely so that the peak of the release function approximated the peak of the current response. In contrast, the inhibitory events are much slower (approximately 2.5 ms 10-90% rise time and 20 ms decay time constant, See Chapter 1 Fig 1.2 and 1.3) so that the current response is a much more blurred version of the release function resulting in the peak of the current response occurring after the peak of the release function.

Maximum light responses do not cause depletion in bipolar cell synapses

The number of quanta released during an excitatory light response can then be compared to the number of vesicles shown to be contained in bipolar cell terminals. This comparison allows one to predict whether these terminals can be depleted during light-evoked neurotransmitter release. Depletion has been postulated to underlie the transience of the transient amacrine and ganglion cells (von Gersdorff and Matthews, 1994; Matthews, 1996; von Gersdorff et al., 1996; von Gersdorff and Matthews, 1997). According to previous studies done in goldfish retinal, each bipolar cell synaptic ribbon holds approximately 110

vesicles. Most likely, these vesicles represent the population that is available for rapid release in response to a light response. Evidence shows that a reserve pool of vesicles does exist that refills the ribbons, but the time constant of this process is on the order of 8 seconds, which is much longer than the duration of either the ON or OFF response in transient amacrine cells.

If each vesicle is equivalent to one quanta, then each bipolar cell ribbon can release 110 quanta. On average, each bipolar cell has 60 ribbons, implying that approximately 6,600 quanta can be release from a single bipolar (von Gersdorff et al., 1996). According to studies in cat, the number of bipolar cell synapses onto ganglion cells ranges from 150 to 540 (McGuire et al., 1986; Freed and Sterling, 1988; Cohen and Sterling, 1990; Cohen and Sterling, 1991). Assuming that amacrine cells receive a similar number of bipolar cell synapses each with a single ribbon, the total number of rapidly releasable vesicles ranges from 16,500 to 59,400. Since even the largest light-evoked response from an amacrine cell in our tiger salamander preparation released less than 2500 quanta, the likelihood of depletion occurring is very low. However, these anatomical findings do not eliminate the possibility that functional depletion occurs before actual anatomical vesicle depletion for some unknown reason.

However, to test directly whether depletion occurs in bipolar cells, we isolated the excitatory inputs by holding amacrine cell at the chloride reversal potential and stimulated the cells with pairs of bright flashes separated by a variable interval. If depletion occurs during the first flash, then the second flash should show a large degree of attenuation. Since the faster response kinetics of

cones, especially in a light-adapted state, allows the flashes to be placed closer together, we used constant green background illumination to inhibit the rod pathway and a red flash to preferentially stimulate the cone pathway. For each cell, we verified that the light flash was inducing a maximal response. Fig 2.6A overlays the responses of a cone to paired flashes separated by 0.5, 1.0, 1.5, and 2.0 seconds. As shown, even when flashes were separated by only 0.5 seconds, the cone responded equivalently to both flashes; therefore, the effects of adaptation to the flashes did not appear to play a significant role under our conditions. However, depletion might occur under different stimulation protocol.

Fig 2.6B shows the current responses of an amacrine cell to the paired flash stimulation, and Fig 2.6C shows the cumulative release function for an amacrine cell stimulated with paired flashes. The initial flash induced the release of 320 quanta on average. The second flash even at an interval of 0.5 seconds could still release 280 quanta. In addition to just the number of quanta, the cumulative release function shows that the time courses of release of the second flashes have approximately the same waveform as the first. The thick line shows the cumulative release function in response to a two-second step of light of the same intensity as the flashes. The function has a similar magnitude and waveform as those for the flash responses, suggesting that approximately the same number of quanta are released during the ON response to the step of light and the flash response under our conditions. Consequently, if depletion does cause the transience during the step of light, then the flash should also deplete the bipolar cell terminals to a certain degree and this depletion would be evident

Fig 2.6: Paired flash stimuli show that bipolar cell terminals are not depleted by light. A) The voltage response of a cone to four pairs of light flashes with interflash intervals of 0.5, 1, 1.5 and 2.0 seconds. The response amplitude was essentially the same at all intervals, providing evidence that retinal adaptation did not significantly affect the cone response under these conditions B) The current response of an amacrine cell to four pairs of to the same set of paired light flashes. In this particular cell, a slight attenuation of the second response was observed for the 0.5 second flash interval. C) By deconvolution methods, a theoretical quantal release function was determined for each flash response. This panel shows the cumulative quantal release curve gotten by integrating those release functions, revealing that this cell released approximately 300 quanta per flash. Even at the shortest interflash interval, little change in the number of quanta occurred between the first and second flashes. D) The bar graph shows the amplitude of the flash responses normalized to the first flash of each pair. These values are averaged over three cells. As with the number of quanta, very little change was observed between the first and second flashes.

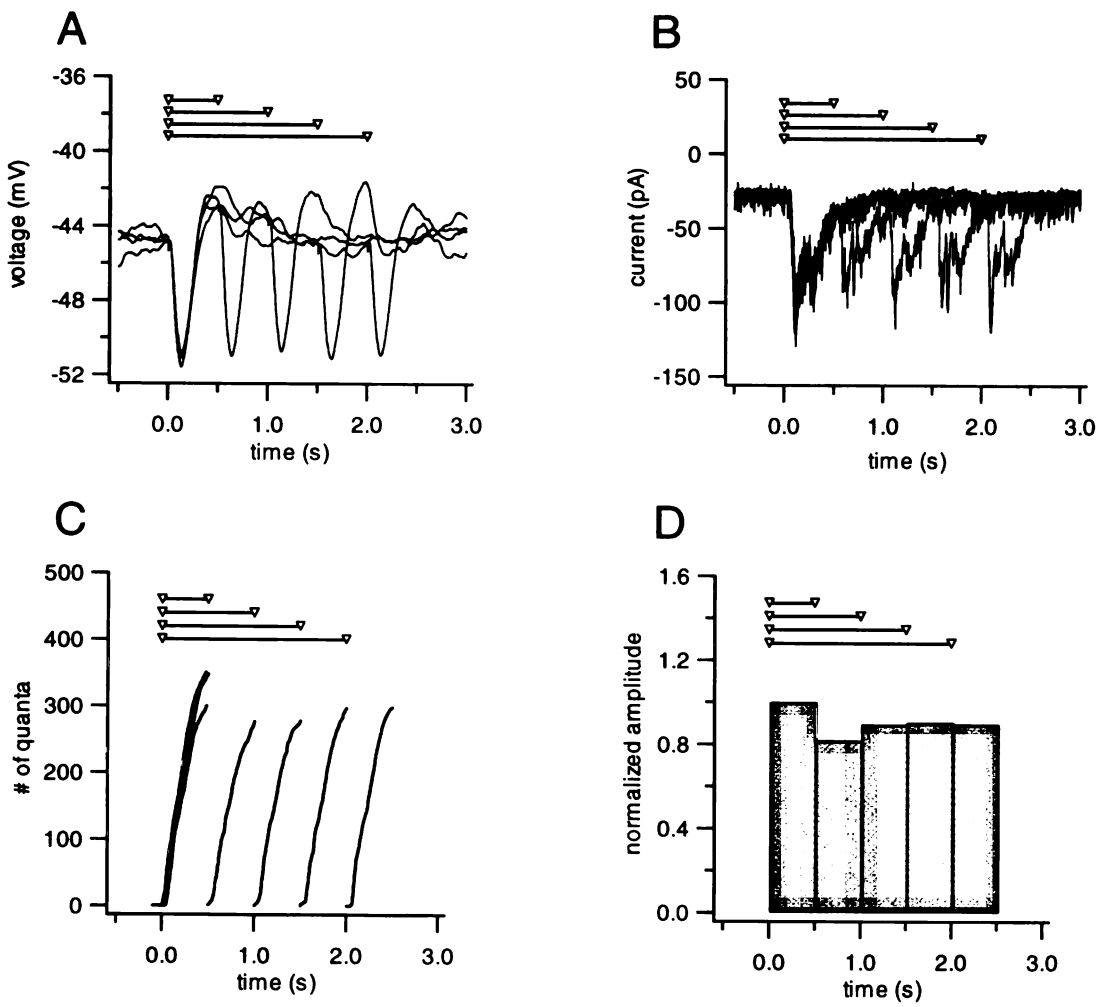
A
-36
-40
-44
-48
-52
voltage (mV)
0.0
1.0
2.0
3.0
time (s)
B
50
0
-50
-100
-150
current (pA)
0.0
1.0
2.0
3.0
time (s)
C
500
400
300
200
100
0
# of quanta
0.0
1.0
2.0
3.0
time (s)
D
1.6
1.2
0.8
0.4
0.0
normalized amplitude
0.0
1.0
2.0
3.0
time (s)

in the second flash since previous work has shown that the time constant of recovery from depletion (approximately 8 s) is much longer than the inter-flash intervals used in our experiments (0.5 to 2 s) (von Gersdorff and Matthews, 1994; Matthews, 1996; von Gersdorff et al., 1996; von Gersdorff and Matthews, 1997). Fig 2.6D shows the normalized peak amplitude of amacrine cell responses to paired flashes from all cells (n=3). Clearly, quantifying the responses by amplitude instead of number of quanta showed the same result of very little decrement.

Discussion

Functional implications of spike-driven multi-quantal neurotransmitter release

The results presented in this study suggest that bipolar cells can simultaneously release multiple quanta of neurotransmitter. This release depends on cadmium-sensitive calcium channels. One possible mechanism is voltage-gated calcium channels allowing the generation of calcium action potentials in bipolar cells, which then initiate multi-quantal release. We found that 2 of 4 cells seemed to have excitatory synaptic inputs that involved multi-quantal release. If calcium spikes do underlie multi-quantal release, then the finding of multi-quantal release in only a subpopulation of bipolar cells would be consistent with previous work showing that calcium spikes were found in only a fraction of bipolar cells (Protti et al., 2000). Functionally, the ability to generate a calcium spike could increase the gain of signal transmission through the bipolar cells. This possibility is only feasible because the resting potential of bipolar cells can be just a few millivolts below the threshold of action potential activation. Consequently, a relatively small input signal could initiate a spike, thus increasing the size of the output signal. Logically, not all the bipolar cells should have the ability to spike because the primarily function of bipolar cells is graded potential signal transmission to maintain a high information rate. However, a subset of bipolar cells adapted to increase signal gain of small signals could be useful in scotopic conditions, when the purpose of the retina is more light detection rather than transmission of detailed visual information. This model is consistent with

the finding that bipolar cells have a higher tendency to fire calcium spikes when they are dark-adapted .

Multi-quantal release from amacrine cells seems to have both sodium and calcium channel dependent components. This finding follows from the amacrine characteristic of using both standard sodium action potential based transmission and graded synaptic transmission. The sodium channels most likely play their usual role of generating sodium action potentials, which allow signals to travel relatively long distances through neuronal processes. However, the calcium channels are primarily located in the synaptic terminal; therefore, their role may be to help amplify whatever signal reaches the terminal rather than to help the signal reach the terminal as for sodium channels.

Light stimuli causes the asynchronous release of quanta

The estimated release function during a light step shown in Fig 2.5 show that the postsynaptic response results from the primarily asynchronous arrival of quanta from presynaptic cells although large responses did involve the virtually simultaneous arrival of a dozens of quanta. Our findings demonstrate that an average light response require the arrival of on the order of one thousand quanta (maximum 2500 quanta). Also, as shown by the release function, the release of the quanta was highly asynchronous, which accounts for the relatively slow rise time of the light response (approximately 50 ms) compared to the 1 ms rise times of the quantal events.

Maximum light responses do not cause depletion of bipolar cell synapses

When the physiological results presented in this study are compared to the anatomical numbers of vesicles and bipolar synapses, the likelihood of synaptic depletion occurring under physiological conditions seems very low even though the numbers used are a mix of findings from amacrine and ganglion cells from tiger salamander, goldfish, and cat. However, a quantum is a functional unit while a vesicle is an anatomical unit. A quantum could theoretically involve the release of multiple vesicles. If we assume that the number of rapidly releasable vesicles ranges from 16,500 to 59,400, then our maximum light-evoked release of 2500 quanta can deplete the vesicle if each quantum contained 6 to 24 vesicles. We cannot rule out this possibility theoretically, but the paired flash experiments showed that even within 0.5 seconds of a saturating light response, the bipolar cell can release an almost equivalent number of quanta during a second flash. This half second interval is much less than the 8 second time constant for refilling bipolar ribbons shown in depletion studies; therefore, we conclude that the ribbons were not depleted.

Our experiments were done with feedback inhibition intact, which as will be shown below plays a strong role in inhibiting the release from bipolar cell terminals. Consequently, it is possible that depletion might be observed if the inhibitory pathways were removed in order to maximize release of vesicles. When we calculated the number of quanta in the light responses from recordings using strychnine and picrotoxin to block inhibition, we found that our largest response (approximately 8000 quanta, data not shown) was over three-fold

larger than the largest response with inhibition intact. Assuming equivalence between one quantum and one vesicle, this number is still much less than the theoretical numbers for depletion of a the synaptic ribbons. It is possible that functional depletion may occur before actual vesicular depletion of the ribbons. However, the previous work showing the effects of depletion showed a strong correspondence between the number of vesicles associated with depletion and the number of vesicles on the synaptic ribbons (von Gersdorff and Matthews, 1994; Matthews, 1996; von Gersdorff et al., 1996; von Gersdorff and Matthews, 1997). In addition, even though the responses are greatly augmented after blocking the inhibitory pathways, this increase in response may not be due to each bipolar cell synapse releasing more vesicles, which would increase the chance for vesicle depletion. Rather, the response increase may be coming from an increase in the number of functional synapses because of the disinhibition of synapses that were almost completely inhibited with feedback intact.

This study is the first study done on amacrine cell spontaneous activity in a slice preparation rather than in culture. The characterization of the amplitude and kinetics of the spontaneous events provide a background for investigating synaptic transmission in the inner retina. For example, the derived quantal response allowed us to reconstruct neurotransmitter release functions of the presynaptic cells in response to a step of light. The release functions for bipolar cells then lead us to show both through calculations and then experimentation that bipolar cell synaptic vesicle depletion does not seem to occur during light responses even though its presence has been shown in isolated bipolar cell

Chapter 3

The circuitry of excitatory input to transient ON/OFF amacrine cells

Introduction

As previously stated, bipolar cells provide the glutamatergic input to amacrine cells. Bipolar cells are divided into two functionally distinct classes. ON-type bipolar cells depolarize in response to light increments while OFF-type bipolar cells hyperpolarize in response to light increments. In other words, in the presence of continuous non-changing background illumination, ON-type bipolar cells are relatively hyperpolarized while OFF-type bipolar cells are relatively depolarized. However, both of these cells release neurotransmitter in response to depolarization. According to this model, then, ON-type bipolar cells should have less spontaneous release than OFF-type bipolar cells. Since the excitatory circuitry of ON/OFF amacrine cells involves synaptic inputs from both types of bipolar cells, they serve as an ideal sensor to test whether OFF-bipolar cells have higher rates of spontaneous release. Since spontaneous activity is essentially the random activity present in the absence of light increments or decrements, the level of spontaneous activity has significant impact on issue of signal-to-noise since any evoked signal has to be received while being blurred by the spontaneous activity.

The transient ON/OFF amacrine cells respond briefly at both the start and end of a continuous step of light. The mechanisms underlying the generation of a transient response during a continuous stimulus are still being delineated.

However, evidence shows that inhibition of $GABA_C$ receptors can increase the duration of amacrine and ganglion cell transient ON responses. (Zhang et al., 1997; Dong and Werblin, 1998; Bieda and Copenhagen, 2000). Since $GABA_C$ receptors are located on bipolar cell synaptic terminals (Lukasiewicz et al., 1994), this finding suggests that a GABAergic amacrine cell circuit working through $GABA_C$ receptors can modulate the release of glutamate. In this study we investigate two new aspects of $GABA_C$ receptor modulation of glutamate release. First, since all the previous work on $GABA_C$ receptors and bipolar cell synaptic transmission has dealt primarily with the ON response of third order cells, we examine the effect of $GABA_C$ receptor on the OFF pathway. Second, in addition to using light-evoked responses, we use spontaneous activity to quantify the glutamate release form bipolar cells without light stimulation and test the effect of $GABA_C$ receptor activation and inhibition on this activity. Using this approach, we can deduce if $GABA_C$ receptor activation acts to hyperpolarize or depolarize the bipolar cells from their resting membrane potential. Since $GABA_C$ receptors gate a predominantly chloride conductance (Lukasiewicz et al., 1994), the result will essentially reveal whether the reversal potential for chloride is more or less depolarized than the resting potential.

Results

A large fraction of excitatory spontaneous input comes form ON-bipolar cells

We isolated excitatory synaptic activity by holding amacrine cells at the chloride reversal. Using a bright two-second flash of light, we clearly identified cells that had transient ON/OFF light responses. APB has been shown to be a potent agonist of the metabotropic glutamate receptor of ON-bipolar cells. The effect of APB is to strongly activate the glutamate receptors, which act through a G-protein pathway to close cationic channels, and thus hyperpolarize the ON-bipolar cell as well as inhibit light responses. As shown in Fig 3.1A, application of 100 uM APB effectively blocked the ON response of amacrine cells to a step of light while leaving a robust OFF-response. The presence of an OFF response also confirmed that OFF bipolar input was intact. Since spontaneous activity is dependent on the membrane potential, the effect of APB should inhibit the spontaneous release of glutamate from ON-bipolar cells. Consequently, we concluded that the effect of APB was limited to the ON pathway. If most of the glutamatergic spontaneous input is from OFF-bipolar cells, then the APB should not have a great effect on the frequency of spontaneous events recorded in amacrine cells. However, Fig 3.1B shows an example of an amacrine cell where APB greatly decreased the spontaneous rate in a reversible manner. As shown by the normalized event frequency graph in Fig 3.1C, this finding was consistent across all cells (n=6). This result implies that a significant fraction of spontaneous activity comes from the ON-bipolar cell. In addition, assuming that the APB-resistant events came from OFF-bipolar cells,

Fig 3.1: A significant portion of the excitatory spontaneous input to ON/OFF amacrine cells come from ON-bipolar cells. Excitatory currents were isolated by recording from amacrine cells in voltage-clamp at a holding potential of -70 mV, the effective reversal potential of the inhibitory currents. A) The light response from a transient ON/OFF amacrine cell to a three second step of light before and after application of APB (100 uM). The arrow points to the inhibited ON response. B) The top trace shows abundant spontaneous activity in control. The middle trace shows a marked decrease in the activity after application of APB. The bottom trace shows that the decrease is reversible. C) The normalized event frequency graph shows that the effect of APB was consistent across all cells (n=5).

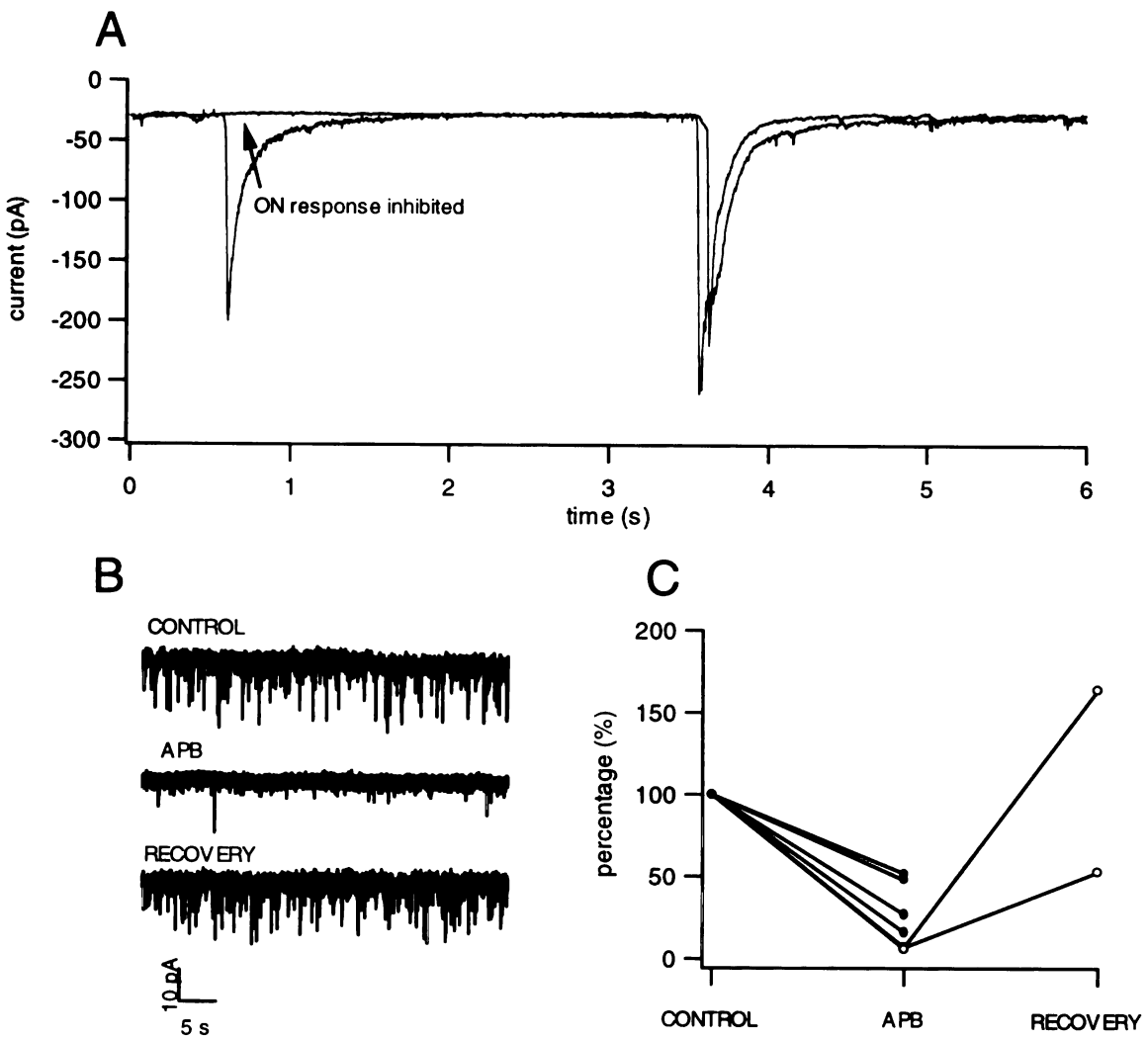
A
0
-50
-100
-150
-200
-250
-300
current (pA)
ON response inhibited
0
1
2
3
4
5
6
time (s)
B
CONTROL
APB
RECOVERY
10 pA
5 s
C
200
150
100
50
0
percentage (%)
CONTROL
APB
RECOVERY

we determined that ON- and OFF-bipolar cell spontaneous events had the same amplitude and kinetics (data not shown).

$GABA_C$ receptors modulate both ON- and OFF-bipolar cells light-evoked release

Excitatory synaptic inputs were isolated by holding transient ON/OFF amacrine cells at near the calculated reversal potential for inhibitory inputs. Strychnine and SR95535 were used to block glycine and $GABA_A$ receptors, respectively. Then, picrotoxin was used to inhibit $GABA_C$ receptors while stimulating the retinal slice with a step of light. As shown in the example in Fig 3.2A, both the ON and the OFF responses of the amacrine cell were potentiated by the inhibition of $GABA_C$ receptors. To quantify the effects of $GABA_C$ inhibition, we calculated the percent increase in charge caused by picrotoxin for both the ON and the OFF responses. The bar graph in Fig 3.2B shows that both the ON and the OFF responses had an increase in charge for all cells (n=5), ranging from 65 to 1900% increase for the ON response and from 29 to 242% increase for the OFF response. This finding indicates that $GABA_C$ modulation occurs at both types of bipolar cells. However, we cannot dismiss possible postsynaptic mechanisms which, for example, might increase the number of apparent events by increasing the sensitivity of the amacrine cell to glutamate.

$GABA_C$ receptor activation hyperpolarizes both ON- and OFF-bipolar cells

The frequency of the events was used to represent the level of glutamatergic release from bipolar cells. Then, the effect of $GABA_C$ activation was examined in two different ways. First, we blocked $GABA_A$ receptors using the antagonist SR95535, and perfused GABA to activate the GABAC receptors.

Fig 3.2: $GABA_C$ modulates light-evoked glutamate release at both the ON and OFF bipolar cells. The excitatory currents of amacrine cells were isolated by holding at a potential of -70 mV, the effective reversal potential of the inhibitory currents. A) This graph shows the light response of an transient ON/OFF amacrine cell to a two second step of light before and after application of picrotoxin (PTX, 200 uM). Both the ON and the OFF responses were augmented by several fold. B) The bar graph shows the percent increase of the ON (open bars) and the OFF (grey bars) response after application of PTX in five different amacrine cells. The values for the ON responses ranged from 65 to 1900%, and the values for the OFF responses ranged from 29 to 242%.

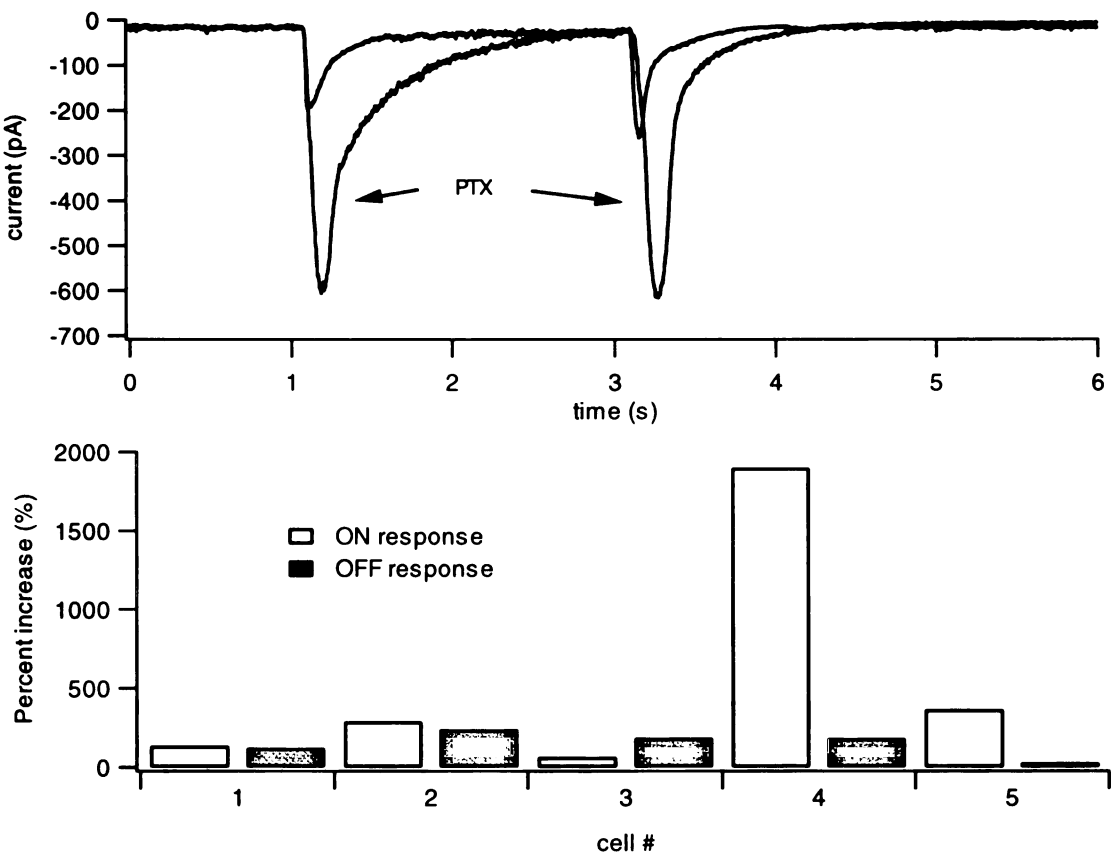
0
-100
-200
-300
-400
-500
-600
-700
current (pA)
PTX
0
1
2
3
4
5
6
time (s)
2000
1500
1000
500
0
Percent increase (%)
ON response
OFF response
1
2
3
4
5
cell #

However, since GABA also could potentially act through $GABA_B$ receptors, we also perfused CACA, a $GABA_C$ receptor-preferring agonist, in order to avoid $GABA_B$ activation. The effect of both of these manipulations was a decrease in frequency of spontaneous excitatory events. Fig 3.3A shows a recording in control, followed by CACA, followed by recovery. Clearly, the frequency of events decreased dramatically in a reversible manner. Fig 3.3B shows the data collected from all cells, showing that the decrease was a very robust effect. This finding suggests that $GABA_C$ activation can inhibit neurotransmitter release from the unstimulated bipolar cell as well as the light-stimulated one. Significantly, blocking the $GABA_C$ receptors with picrotoxin had no statistically-significant effect on the spontaneous rate, indicating that $GABA_C$ receptors are not tonically activated to a significant degree (data not shown).

Since our results suggested that many of the spontaneous events resulted from ON-bipolar cell input, we tested to see if $GABA_C$ still caused a decrease in spontaneous frequency after APB was used to inhibit ON-bipolar cell spontaneous release. In our model, the remaining events should be predominantly from the OFF-bipolar cell inputs. As shown in by the raw data traces in Fig 3.4A, APB caused a decrease in the frequency of spontaneous excitatory events. Then, the additional perfusion of CACA decreased the frequency even further. This result was consistent across all cells (n=3) as shown by the normalized frequency graph in Fig 3.4B.

Fig 3.3: $GABA_C$ modulates the spontaneous release of glutamate from bipolar cells. The excitatory currents of amacrine cells were isolated by holding at a potential of -70 mV, the effective reversal potential of the inhibitory currents. A) The top trace shows the spontaneous activity recorded in control solution. The middle trace shows that this activity is decreased substantially by the application of the $GABA_C$ receptor agonist, CACA. The bottom trace shows that the decrease is reversible. B) The normalized event frequency graph shows that the effect of $GABA_C$ receptor activation was consistent across all cells (n=7). In four cells, CACA was used to activate $GABA_C$ receptors. In three cells, GABA in the presence of the $GABA_A$ antagonist SR95535 was used to activate the $GABA_C$ receptors preferentially.

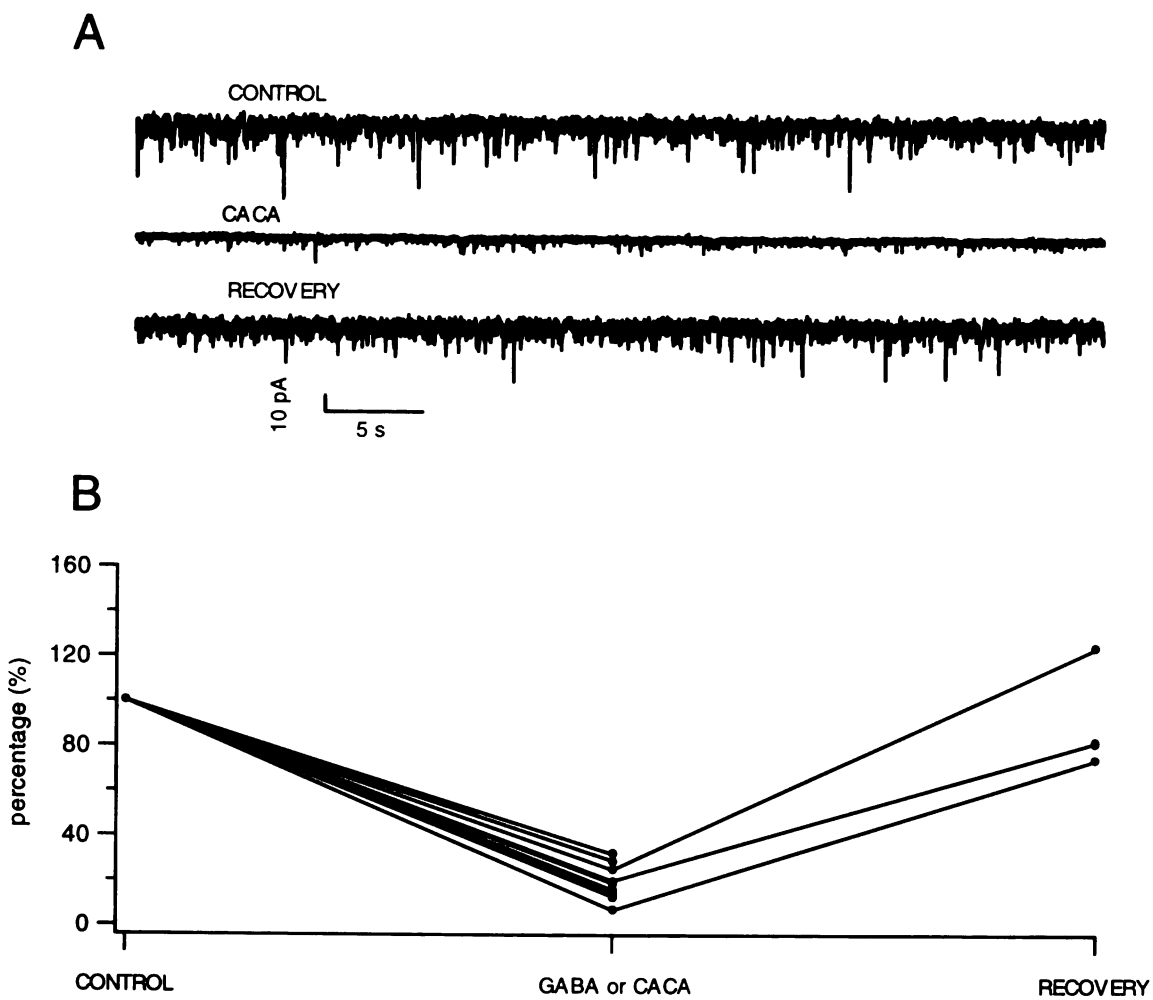
A
CONTROL
CACA
RECOVERY
10 pA
5 s
B
160
120
80
40
0
percentage (%)
CONTROL
GABA or CACA
RECOVERY

Fig 3.4: $GABA_C$ receptor activation decreased the spontaneous release from OFF-bipolar cells. The excitatory currents in amacrine cells was isolated by holding at -70 mV, the effective reversal potential of the inhibitory currents. A) The top trace shows the spontaneous activity in control solution. The middle trace shows that APB decreases the spontaneous rate, presumably blocking the events from ON-bipolar cells and leaving mainly OFF-bipolar cell mediated events. The bottom trace shows that $GABA_C$ receptor activation by CACA decreases the spontaneous rate even further, consistent with inhibition of the OFF-bipolar cell spontaneous release. B) The normalized event frequency graph shows that the additional effect of CACA on spontaneous rate after APB was consistent across all cell (n=3). In the lowest trace on the graph, APB so strongly inhibited that frequency of spontaneous events that the additional percentage decrease in frequency due to application of CACA is subtle.

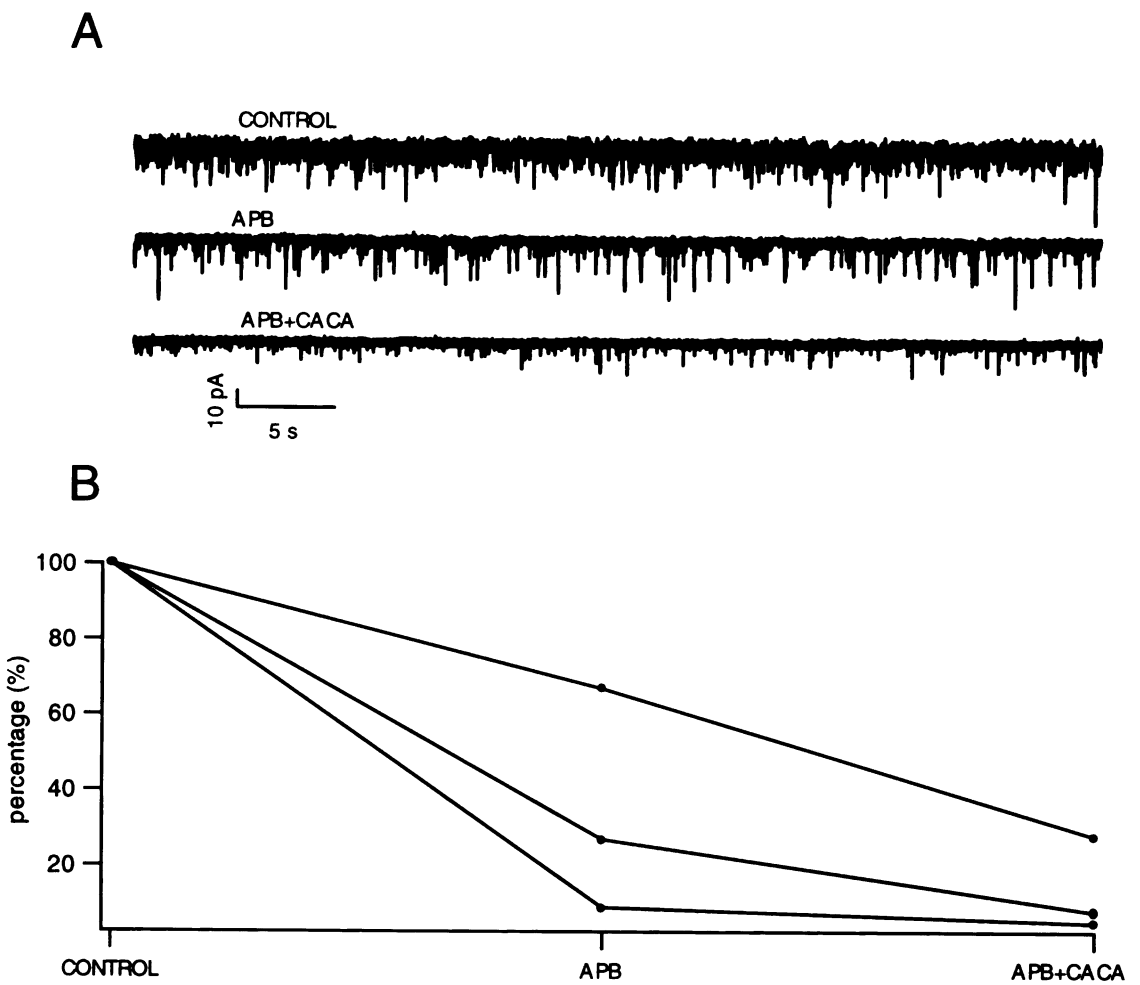
A
CONTROL
APB
APB+CACA
10 pA
5 s
B
100
80
60
40
20
percentage (%)
CONTROL
APB
APB+CACA

Discussion

Both ON- and OFF-bipolar cells provide spontaneous input to amacrine cells

Our results showed that under our conditions that a significant fraction of spontaneous glutamatergic spontaneous input to transient ON/OFF amacrine cells comes from ON-bipolar cells. One model that explains our findings stems from the use of dim ambient light during the slice preparation. Perhaps in a totally dark-adapted retina, the ON-bipolar cell spontaneous release would be extremely low in order to optimize photon detection. However, under our conditions, the retina is most likely light-adapted to some degree. In this case, maybe a higher rate of spontaneous ON-bipolar release allows the ON pathway to convey information during light decrements through decreases in the spontaneous rate and allow better termporal resolution. Similarly, in a totally dark-adapted retina, when photon detection is the primary goal, OFF-bipolar cells may maintain a high rate of spontaneous release so that they can convey information about light increments by decreasing their spontaneous release. In fact, responses to light decrement in dark-adapted retina are minimal. In contrast, in a more light-adapted retina, the main function of the OFF-bipolar cell is to signal light decrements.

$GABA_C$ modulates both ON- and OFF-bipolar cell synaptic release

Clearly, $GABA_C$ receptors play an important role in modulating glutamate release. Blocking $GABA_C$ increased the amount of charge carried by glutamate-driven responses in amacrine cells. This increase in response was found in both the ON (65 to 1900%, Fig 3.2B) and the OFF (29 to 242%, Fig 3.2B) responses

to steps of light, indicating that $GABA_C$ receptors act similarly on both the ON and OFF bipolar cells. Release from both ON and OFF bipolar cells was inhibited by $GABA_C$ activation indicating that the reversal potential of these receptor channels is more hyperpolarized than the resting membrane potential of bipolar cells under our conditions. Statistically, blocking $GABA_C$ receptors did not have any effect on the rate of glutamatergic spontaneous events, indicating that basal activation of $GABA_C$ receptors was low. In other words, the primary role of these receptors occurs during light-evoked response rather than during unstimulated conditions.

Chapter 4

Automated detection and analysis of spontaneous post-synaptic currents

Introduction

Chemical synaptic transmission in the nervous system is mediated by the impulsive release of individual "packets" of neurotransmitter from presynaptic terminals. The resultant binding of transmitter molecules from a single packet to receptors on postsynaptic cells gate ionic channels that generate membrane conductance changes having onsets of ~1 ms and decays from peak ranging from a few to tens of milliseconds. Electrophysiological recording from postsynaptic cells often reveals a sustained barrage of spontaneous synaptic events. The timecourse and amplitude of these spontaneous events reflect receptor channel kinetics and the rates of neurotransmitter release and clearance. Differences in these properties can be used to identify the specific classes of synaptic inputs to a neuron (Rorig and Grantyn, 1993). Moreover, the waveform of the events represents the basic unit, or quantal event, of which larger evoked responses are comprised.

To estimate accurately and reliably the parameters of the quantal events requires recording hundreds or thousands of events over periods of many minutes to hours. Although the detection of these events can be done visually, automatic detection and analysis of spontaneous events greatly increases the number of events that can be analyzed and reduces the time required. In addition, automated algorithms unambiguously define the selection criteria,

making the detection and characterization more objective and repeatable from data set to data set.

We were faced with the problem of analyzing spontaneous events resulting from the random activation of glutamate-, GABA-, and glycine-gated mediated synaptic inputs onto single retinal ganglion cells. We wanted to detect and characterize each type of event after isolation by pharmacology and holding potential manipulation. In addition, we wanted to compare the level of excitatory and inhibitory spontaneous synaptic input into each cell without using pharmacological or voltage-clamp manipulations. Using these techniques would affect the presynaptic circuitry and therefore alter the input levels we wanted to measure (Tian et al., 1998). However, preliminary data revealed that inhibitory events had a much slower decay phase than excitatory events. Consequently, we needed a program that not only could detect and characterize events reliably but also could discriminate between the different types of events by taking advantage of differences in kinetics.

Several different approaches to automated detection were investigated and found to be less than optimal for our purposes. Most detection algorithms fall into three basic categories: those based on an amplitude threshold (Liu and Kim, 1983; Bergman and DeLong, 1992; Cochran, 1993; Dempster, 1993; Bykhovskaia et al., 1996; Carlson and Krieger, 1996), those based on a first derivative threshold (Morales et al., 1985; Cocatre-Zilgien and Delcomyn, 1990; Ankri et al., 1994), and those based on template comparison (Salganicoff et al., 1988; Yang and Shamma, 1988; Yamada et al., 1992; Oghalai et al., 1994;

Clements and Bekkers, 1997). Using an amplitude threshold is intuitive but suffers from being sensitive to baseline drift; therefore the more robust versions of the algorithm, such as the one in this study, include baseline compensation strategies (Liu and Kim, 1983; Bergman and DeLong, 1992; Cochran, 1993; Bykhovskaia et al., 1996; Carlson and Krieger, 1996). Using a first derivative threshold has the advantage of being insensitive to baseline drift but has the disadvantages of being sensitive to high frequency noise and of having a less intuitive choice for the threshold (Morales et al., 1985; Cocatre-Zilgien and Delcomyn, 1990; Ankri et al., 1994). More successful implementations of this approach benefit from smoothing to reduce high-frequency noise. Finally, using a template comparison usually has high sensitivity to events that match the template. However, the method depends on knowing in advance the waveform of the synaptic events of interest, and it loses sensitivity dramatically if the actual event waveforms differ moderately from the template waveform (Clements and Bekkers, 1997). In addition, analysis of data that includes events that overlap or multiple populations of events, each with different kinetics, is problematical.

In this paper, we describe an automated program that uses a modified version of the amplitude threshold algorithm to detect synaptic events. Simulations show that the program achieves high sensitivity with a low false positive rate and provides accurate estimates of event amplitudes and kinetics. In addition, the program can reveal the presence of two populations of kinetically distinct events in a recording trace. This program was successfully used to

Methods

We created the software for detecting and analyzing synaptic events using the programming language supported by the data analysis package IGOR Pro (Wavemetrics, Lake Oswego, OR). The event detection program will be available for download at the IGOR Pro website, www.wavemetrics.com, under the name "Minifit." IGOR Pro is compatible with both Macintosh and PC systems and can import data from any acquisition software that can export files in text or binary formats. In addition, third party applications such as Data Access (Bruxton Corporation, Seattle, WA) allow direct loading of files from such common applications as Pulse (Heka eletronik), pClamp (Axon Instruments), and Acquire (Bruxton Corporation).

Event Detection

When analyzing a recorded trace with spontaneous events, the program makes three passes through the data. During the first pass, it generates a list of potential event start and peak time points. Each of these points is either a local maximum or a local minimum. The software defines a local maximum as a point with a zero first derivative and a negative second derivative and defines a local minimum as a point with a zero first derivative and a positive second derivative. The list basically alternates between local maxima and minima (Fig 4.1A). For downward events, each local minimum is a potential peak with the preceding local maximum as the event start. For upward events, each local maximum is a potential peak with the preceding local minimum as the event start. During the second pass, the program eliminates the events that do not exceed the selected

Fig 4.1: The three stages of synaptic event detection. A) The first stage is to locate all local maximums and minimums in the recording trace. The top trace is an actual current recording with a single downward-going synaptic event, and the bottom trace is the first derivative of the recording. The upward arrows on the top trace signify local maximums, and the downward arrows signify local minimums. The vertical dashed lines show how these local maximums and minimums correspond to where the first derivative equals zero. At this stage, each local minimum is the peak of a potential synaptic event with the immediately preceding local maximum as the event start. B) The second stage is to remove noise events by an amplitude threshold screen. The trace is the same as the top trace in panel A. The vertical bar represents the threshold setting of the program (2 pA for this study). All synaptic events that do not have an amplitude that exceeds this threshold are removed from consideration. The amplitude is defined simply as the difference between the value at the start and peak time points. The start and peak time points for the remaining potential event are marked by arrows. C) The third stage is to confirm that the selected events actually exceed threshold by using averaging to determine a more accurate amplitude. Again, the trace is the same as the top trace in panel A. The amplitude is recalculated as the difference between the average baseline value (horizontal line marked with an arrow) and the average peak value (horizontal line marked with an arrow). If this amplitude value does not exceed the threshold criterion, then the event is removed from consideration.

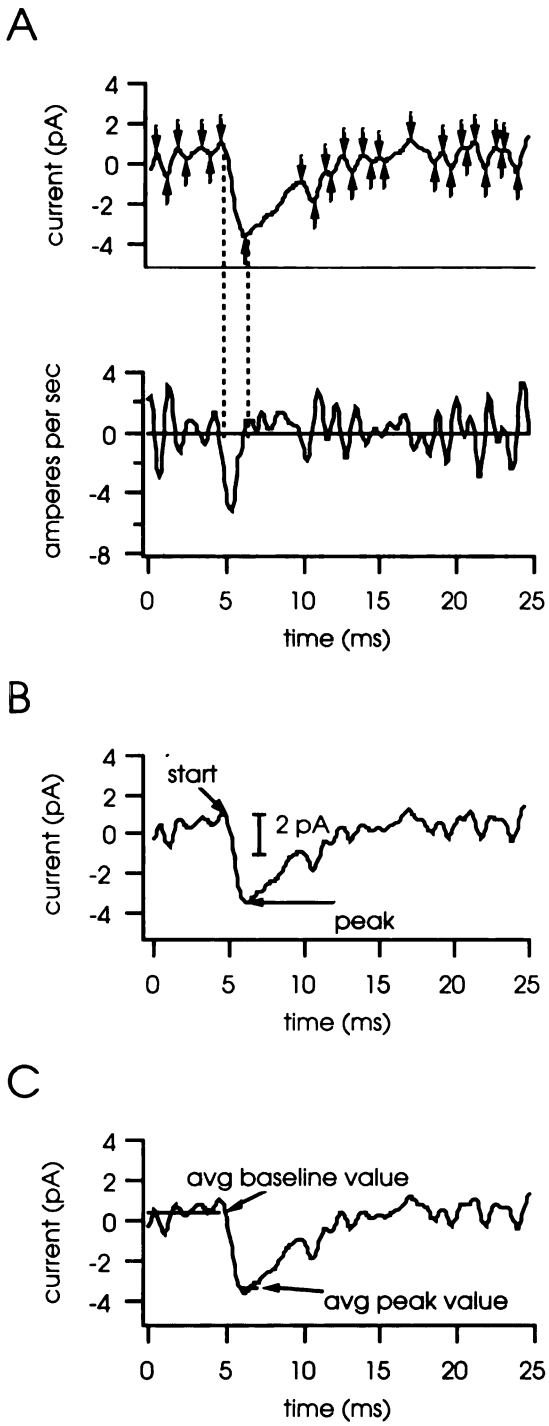
A
current (pA)
4
2
0
-2
-4
amperes per sec
4
0
-4
-8
0
5
10
15
20
25
time (ms)
B
current (pA)
start
2 pA
peak
time (ms)
C
current (pA)
avg baseline value
avg peak value
time (ms)

amplitude criterion (2 pA was found to be optimal for the simulated data in this study) (Fig 4.1B). The program computes the amplitude as the difference between the start and the peak of each potential peak. If the difference is less than the user-set criterion value, then the software removes those start and peak time points from the list. During the third pass, the program averages a segment preceding the start point (5 ms here) and a segment following the peak point (0.5 ms here) to remove noise from the data in order to determine the amplitude more precisely. The recalculated amplitude equals the difference between these two averages (Fig 4.1C). Again, if the amplitude is less than the user-defined criterion value, those start and peak time points are removed from the list. The remaining entries serve as the final set of detected events, and the recalculated amplitudes serve as the outputted amplitude values for those events. The program places a symbol on the start and peak time points of each event to facilitate visual inspection of the program results.

If high frequency noise corrupts the onset phase of an event, the basic detection algorithm described above may miss the true start of the event. To deal with the problem of high frequency noise, the program allows the user to low-pass filter the data using the fast Fourier transform (IGOR Pro).

Event characterization

The program not only detects events, which enables one to determine their frequency, but also analyzes the kinetics of the discrete events detected. The 10-90% rise time was selected to describe the kinetics of the onset phase of an event. For analysis of the decay phase, the program fits both a single and a

double exponential curve to the decay phase of each discrete event and uses the calculated decay time constants as a measure of the kinetics. The Levenberg-Marquardt non-linear curve-fitting algorithm (IGOR Pro) was used to do the fitting. Instead of fitting the same number of points for each event (Ankri et al., 1994), the program determines the end of the event by marking the time where the trace returns to the baseline value. A sliding box average of adjustable length (1 ms for this study) reduced the noise during this calculation. The program then fits all the data points between the peak and end time points. The software displays the distribution and cumulative probability distribution for each calculated parameter and also outputs the means and modes of the distributions. In addition, the user can choose to overlay the single exponential fit, the double exponential fit, or the better of the two fits on each event for visual inspection.

The software uses the adjusted R^2-statistic to determine whether a double exponential curve fits significantly better than a single exponential curve. Since the double exponential curve is the sum of two single exponential curves, many measures of goodness-of-fit will indicate that fitting with a double exponential curve is always equal to or better than a single exponential curve. However, the adjusted R^2-statistic determines whether the improvement in the fit with the double exponential curve is more than expected simply from the increase in the number of fitting parameters (Glantz, 1990).

The program also computes an average waveform by performing a point-by-point average of all the discrete events detected. The events are aligned at the midpoint of the onset phase. This average reduces the noise so that an

alternative measure of the amplitude and kinetics can be computed from the average waveform. However, if two different classes of synaptic events occur concurrently in the data, then the average waveform would by a hybrid of the two types and not be an accurate estimate of the true waveform of either one.

The start, peak and end time points for each event as well as its amplitude, decay time constant, and 10-90% rise time are stored in individual arrays. Although these arrays can be exported in text or binary format, they are meant primarily for use within IGOR Pro. For analysis, IGOR Pro provides a wide range of functions, such as curve fitting, correlation, binning, and statistical tests, as well as graphing options, such as category plots and 3D graphs. Since the data are saved in user-accessible arrays, users can perform any analyses that fit their specific needs. For example, to investigate whether dendritic filtering had a significant effect on the results, one can test for correlation between the decay time constants and the amplitudes by creating an XY plot, doing a linear regression, and then determining the correlation coefficient. By default, the program creates histograms and cumulative probability distributions of the amplitude, time-to-peak, and decay time constant as well as an event frequency versus time graph and a point-by-point average waveform.

Simulations

We quantified the performance of the algorithm by testing the program on simulated traces containing idealized synaptic events added to noise. To create realistic noise, we used "pink" noise with a power spectrum that falls off as

$(1 + \frac{300}{\text{frequency}})$ as previously described (Clements and Bekkers, 1997). Fig 4.2A shows that the power spectrum of our simulated noise matches that of actual noise from recordings of mouse ganglion cells (Tian et al., 1998). To show that the performance of the program does not depend on the noise power spectrum, we also ran simulations using "white" noise, which has a flat power spectrum. The simulated events followed a time course based on the product of two exponential curves as described below:

$$i(t) = A*(1-e^{-\frac{t}{ONSET}})*e^{-\frac{t}{DECAY}}, \qquad (1)$$

where ONSET and DECAY are the time constants for the onset and decay phases respectively. We adjusted the value of the variable *A* so that the peak value equaled the desired event amplitude. To simulate excitatory postsynaptic currents (EPSCs) which have fast kinetics, we used an ONSET of 1 ms and a DECAY of 4 ms (Tian et al., 1998). These values yield an event with a total time-to-peak of 1.6 ms (10-90% time-to-peak = 0.88 ms) and a decay of 4 ms (Fig 4.2B). Each simulated data trace had a total length of 201 s with a sampling frequency of 10 kHz. Using a sampling frequency of 10 kHz minimized event distortion due to the fast rising phase. For testing the sensitivity of the program to discrete events, we generated traces with a simulated event every 200 ms and a total of 1000 events per trace. For testing the sensitivity of the program to overlapping events, we generated traces with a second event added to each discrete event, shifted by a variable delay time (1 to 15 ms), to make a total of 2000 events. All simulated noise had an amplitude standard deviation of 1 pA so

Fig 4.2: Comparison of real and simulated data. A) The power spectrum of the simulated noise matches the power spectrum of actual recording noise. The top trace shows the power spectrum of the simulated noise, which falls off as $1+(\frac{300}{f})$. The bottom trace shows the power spectrum of actual noise from a recording from a mouse retinal ganglion cell. The power spectrum was taken from a segment of the recording that had no obvious synaptic events. B) The simulated fast synaptic events match real EPSCs. The top trace shows an example of the standard simulated fast synaptic events used (ONSET = 1 ms, DECAY = 4 ms – See Eqn 1). The bottom trace shows an EPSC from a recording from a mouse retinal ganglion cell.

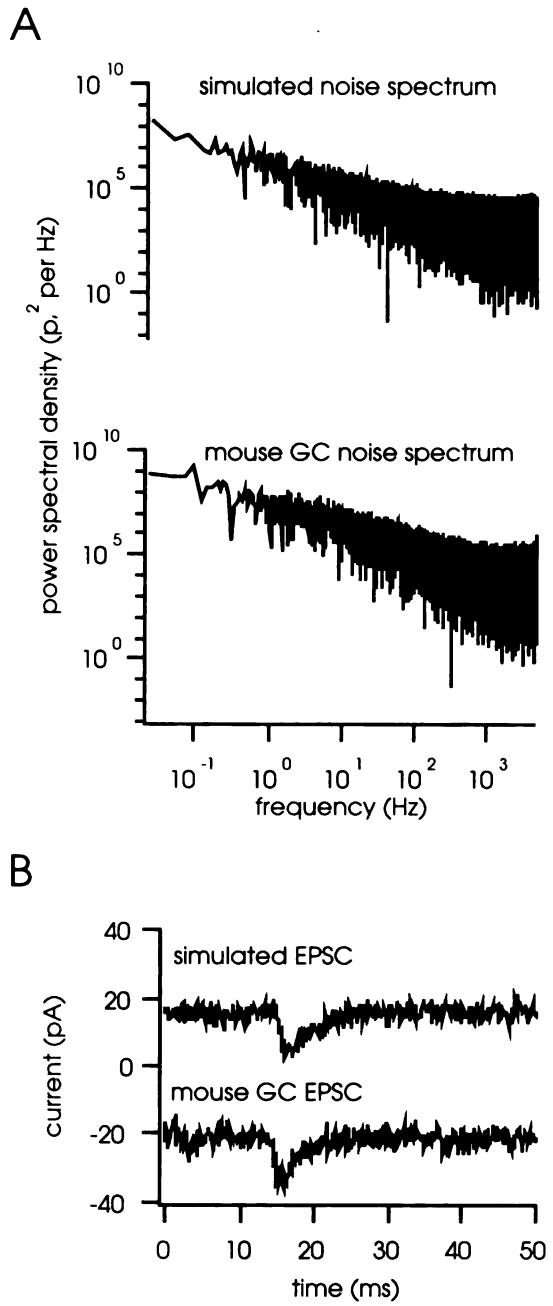
A
simulated noise spectrum
mouse GC noise spectrum
power spectral density (p.A^2 per Hz)
frequency (Hz)
B
simulated EPSC
mouse GC EPSC
current (pA)
time (ms)

that the amplitude of events and the amplitude criterions discussed in this study can equivalently be interpreted as signal-to-noise ratios instead of pA. Our recordings from retinal ganglion cells contained noise with amplitude standard deviations of less than 1 pA (Tian et al., 1998).

Results

The performance of the program was characterized by two values: the sensitivity, defined as the percentage of true events detected, and the rate of false positives, defined as the number of false events detected per second. Clearly, the ultimate goal was to obtain a high detection level with a low false positive rate by adjusting the parameters of the program. The critical program parameters inputted by the user are the amplitude criterion and the cut-off frequency for the Fourier Transform low-pass filter. The first section of the results describes how the values for these two parameters were selected and how well the program performed on discrete events with those settings. The second section describes the effect of overlapping events on the performance. The third section examines how well the program detected events with different kinetics. Finally, the fourth section shows the accuracy with which the program estimated the true values for the amplitude and kinetics of events.

Selection of program settings and performance on discrete synaptic events

We ran the program on traces containing 3 pA events (ONSET = 1ms, DECAY = 4ms) using low-pass cut-off frequencies ranging from 2000 Hz to 50 Hz. Using frequency cut-offs of 1000 Hz or less, the sensitivity increased to almost 100% and the false positive rate decreased to nearly zero. Consequently, we set the frequency cut-off to 1000 Hz to examine the sensitivity and false positive rate of the program as a function of the amplitude criterion setting (range: 1.75 to 3.0 pA). We used the program to analyze four different traces, containing either one thousand 2, 3, 4, or 5 pA events. As Fig 4.3A shows, an

amplitude setting of 2 pA resulted in a detection rate of almost 100% for event amplitudes at or above 3 pA and 61% for 2 pA events. In addition, the sensitivity remained high even when the events were placed on "white" noise (open circles) instead of "pink" noise. Fig 4.3B shows the false positive rate for the trace with the highest false positive rate at each threshold setting. At the same amplitude threshold of 2 pA, the false positive rate was only 0.07 per sec in both "pink" (filled circles) and "white" (open circles) noise. From these results, we decided to use a threshold setting of 2 pA and a frequency cut-off of 1000 Hz for the remainder of the simulations discussed below.

Effect of overlapping events on performance

Although the algorithm worked well on discrete events, neurons that have a high level of spontaneous synaptic input often have events that overlap. To calculate an accurate event frequency requires reliable detection of overlapping events as well. Consequently, we tested the program on simulated overlapping EPSCs (total time-to-peak = 1.6 ms; 10-90% time-to-peak = 0.88 ms; decay time constant = 4 ms) with amplitudes ranging from 3 to 5 pA. The adjusted delay between two overlapped events ranged from 1 to 15 ms. As Fig 4.4 shows, when events are separated by only 1 ms, which is less than the total time-to-peak of the events, the program only finds 50% of the peaks because each pair of overlapped peaks looks like a single peak with twice the amplitude. Previous algorithms have used inflection points on the onset phase of events to detect such closely spaced events (Ankri et al., 1994; Bykhovskaia et al., 1996; Carlson and Krieger, 1996), but we did not feel that these occurrences could be reliably

Fig 4.3: Effect of threshold setting on sensitivity and false positive rate. A simulated trace containing one thousand excitatory events (total time-to-peak = 1.6 ms; 10-90% time-to-peak = 0.88 ms; decay time constant = 4 ms) over 201 seconds with a noise standard deviation of 1 pA was analyzed for event amplitudes ranging from 3 to 5 pA. The program used threshold criteria ranging from 1.75 to 3 pA and a frequency cut-off of 1000 Hz. A) Each curve shows the percentage of events detected using a different threshold criterion ranging from 1.75 to 3 pA. The sensitivity increased as the threshold criterion was decreased and as the event amplitude increased. The filled symbols show the results using "pink" noise, and the open circles show the results using "white" noise. The sensitivity was high regardless of the type of noise. B) The false positive rate increased as the threshold setting was decreased. The false positive rate shown is the highest false positive rate encountered at a given threshold setting. The filled circles show the results using "pink" noise and the open circles show the results using "pink" noise. The false positive rate was low regardless of the type of noise.

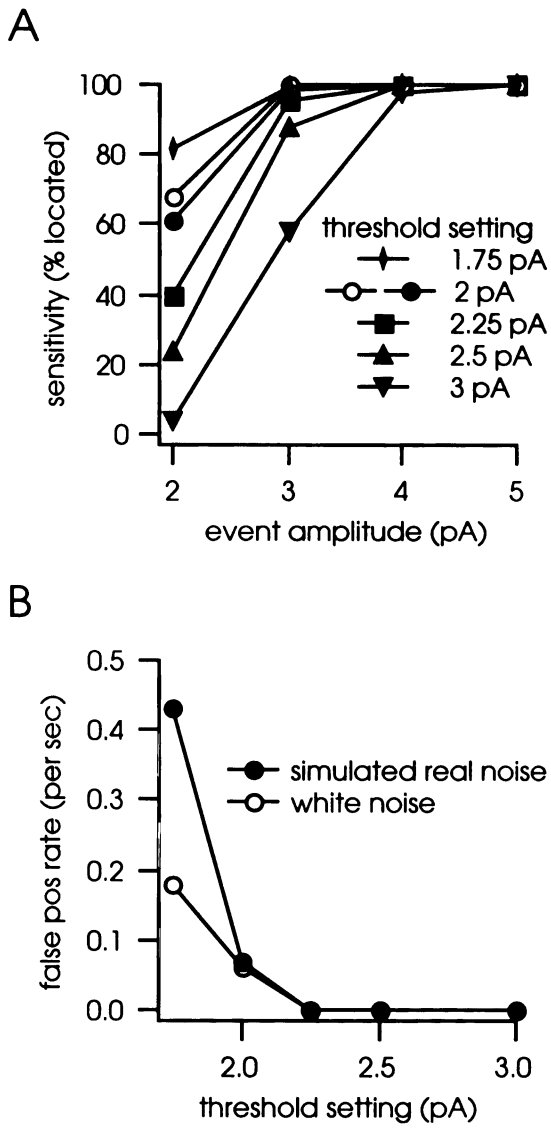
A
100
80
60
40
20
0
sensitivity (% located)
threshold setting
1.75 pA
2 pA
2.25 pA
2.5 pA
3 pA
2
3
4
5
event amplitude (pA)
B
0.5
0.4
0.3
0.2
0.1
0.0
false pos rate (per sec)
simulated real noise
white noise
2.0
2.5
3.0
threshold setting (pA)

distinguished from noise. However, at 2 ms separation, detection rates of events of all amplitudes tested exceeded 80%; and at 3 ms separation, detection increased to almost 100% for 4 and 5 pA events. Significantly, the false positive rate remained at 0.07 per second or less (data not shown). These results show that the program has good sensitivity to overlapping events separated by 2 ms or more without sacrificing specificity to real events.

Effect of event kinetics on performance

Because all the simulated events thus far discussed have had the same time course, we examined the effect of altering the onset and decay kinetics on detection performance. Fig 4.5A shows that changing the decay time constant from 4 ms to 25 ms actually improved the detection of 2 pA events by a few percent while detection of 3 to 5 pA events remained at nearly 100%. Increasing the total rise time from 1.0 to 3.2 ms decreased the sensitivity to only 2 pA events significantly (~10%) with little effect on detection of 3 to 5 pA events. However, the false positive rate increased with increasing time-to-peak especially for 5 pA events, where the false positive rate increased from 0.07 to 0.43 per second (Fig 4.5B filled circles). The increase resulted from the mistaken identification of a secondary event occurring during the prolonged onset phase. Consequently, these false positives were dependent on the frequency of events rather than simply time. In other words, the program still had a baseline false positive rate of 0.07 per second but had an additional false positive rate of 0.072 per event (0.36 per second/5 events per second), which is only a 7.2% error. Significantly, by lowering the frequency cut-off for the Fourier Transform low-pass filter from 1000

Fig 4.4: Effect of overlapping events on sensitivity. A simulated traces containing one thousand pairs of overlapping excitatory events (total time-to-peak = 1.6 ms; 10-90% time-to-peak = 0.88 ms; decay time constant = 4 ms) over 201 seconds with a noise standard deviation of 1 pA was analyzed for event separation times ranging from 1 to 15 ms and event amplitude ranging from 3 to 5 pA. The program used a threshold criterion of 2 pA and a frequency cut-off of 1000 Hz. Each trace shows the sensitivity to overlapped events of a different amplitude. Sensitivity increased with increasing separation time, exceeding 80% by 2 ms separation. Sensitivity also was better for events with larger amplitude.

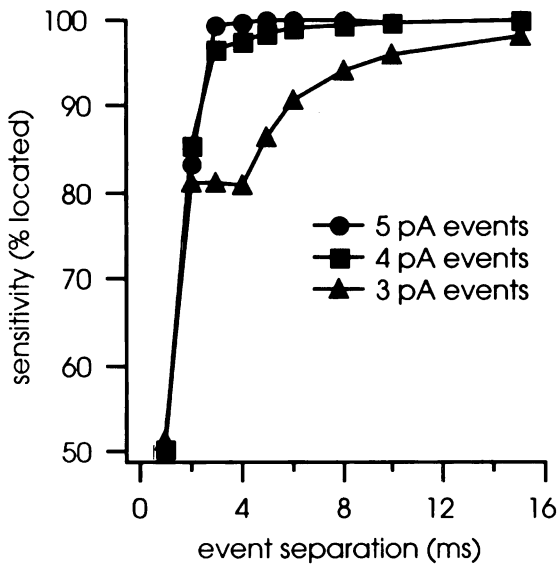
100
90
80
70
60
50
sensitivity (% located)
0
4
8
12
16
event separation (ms)
5 pA events
4 pA events
3 pA events

Fig 4.5: Effect of event kinetics on sensitivity and false positive rate. A simulated trace containing one thousand events over 201 seconds with a noise standard deviation of 1 pA was analyzed for event amplitudes ranging from 2 to 5 pA, times-to-peak ranging from 1.0 to 3.2 ms, and decay time constants of 4 and 25 ms. The program used a threshold criterion of 2 pA and a frequency cut-off of 500 or 1000 Hz. A) Each trace shows the sensitivity to events with different kinetics. Variations in kinetics did not have any effect on the sensitivity for events larger than 3 pA. For 2 pA events, small differences were seen in the sensitivity. B) The open circles show the results using a frequency cut-off of 1000 Hz. The false positive rate increased with increasing time-to-peak. The filled circles show the results using a frequency cut-off of 500 Hz. The lower frequency cut-off removed the extra false positives caused by the increasing time-to-peak. Only the results from traces containing events with a decay time constant of 4 ms were included, and the false positive rate shown was the highest rate encountered at a given time-to-peak.

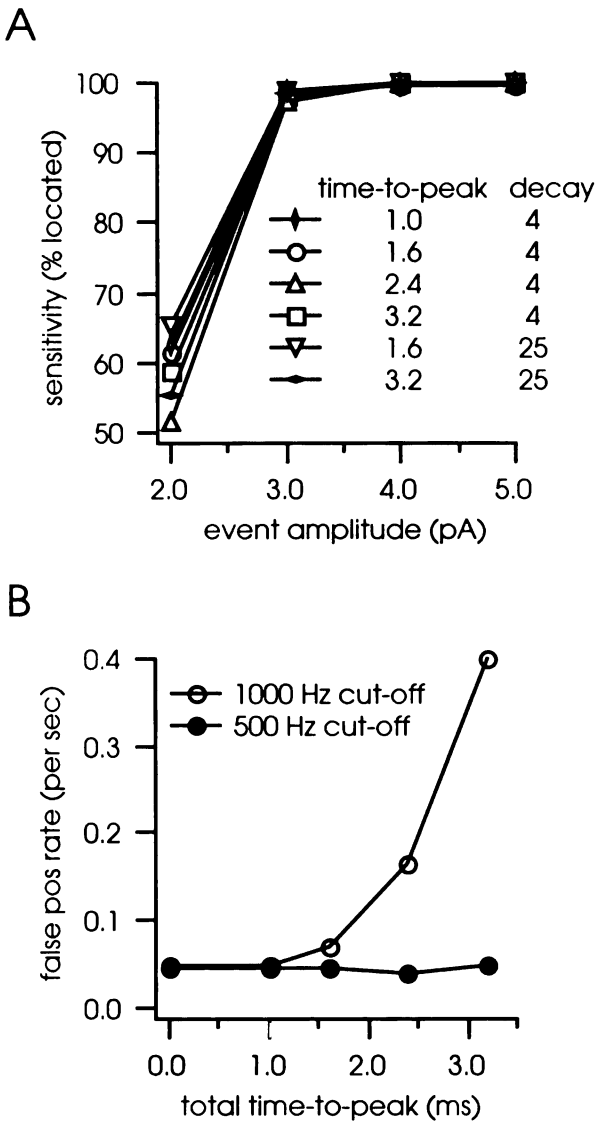
A
100
90
80
70
60
50
sensitivity (% located)
time-to-peak decay
1.0 4
1.6 4
2.4 4
3.2 4
1.6 25
3.2 25
2.0
3.0
4.0
5.0
event amplitude (pA)
B
0.4
0.3
0.2
0.1
0.0
false pos rate (per sec)
1000 Hz cut-off
500 Hz cut-off
0.0
1.0
2.0
3.0
total time-to-peak (ms)

to 500 Hz, one can remove the extra false positives created by the extended time-to-peak (Fig 4.5B open circles).

Accuracy of the waveform characterization

To verify that the program accurately determines the amplitude and kinetics of the events, we examined the estimates for amplitude, decay time, and 10-90% time-to-peak for a fast event (10-90% time-to-peak = 0.88 ms, decay = 4ms). Three different measures describe each parameter - the arithmetic mean, the mode of the Gaussian curve fit to the distributions, and the value determined by analyzing the point-by-point average wave. In general, all three measures accurately matched the actual value of the amplitude (Fig 4.6A), the time-to-peak (Fig 4.6B) and decay time constant (Fig 4.6C). However, the mean value for the decay time constant of the fast event tended to overestimate the true value. This overestimation occurred because the decay time distribution was skewed toward larger values due to the proximity to zero (Fig 4.7B, left distribution). Distributions that are not affected by the zero limit (Fig 4.7B, right distribution) are more symmetrical, and in those cases, the mean is a more accurate estimate of the true value.

By combining the ability to detect events of different amplitude and kinetics with the ability to accurately determine those parameters, the program can separate different kinds of events based on their waveform. In Tian et al (1998), voltage-clamp recording at a holding potential of –70 mV contained both excitatory glutamate-mediated and inhibitory GABA/glycine-mediated events. Since the inhibitory events had a much longer decay than the excitatory events,

Fig 4.6: Estimation of event amplitude, decay time constant, and 10-90% time-to-peak. A simulated trace containing one thousand excitatory events (amplitude = 5 pA, decay time constant = 4 ms, 10-90% time-to-peak = 0.88) was analyzed using a threshold setting of 2 pA and a frequency cut-off of 1000 Hz. Each event parameter was estimated in three ways, namely the arithmetic mean (circles), the mode of the Gaussian curve fit to the parameter distribution (square), and the value derived from the average waveform (triangle) A) All three measures estimated the amplitude accurately although some overestimation occurred for 2 pA events. B) The mode and the average waveform value accurately estimated the true decay time constant value of 4 ms for all amplitudes. The mean tended to overestimate the decay time constant because of the skew of the distribution toward larger values due to the proximity to zero. C) All three measures accurately estimated the 10-90% time-to-peak of 0.88 ms for events larger than 4 pA. Some error occurred for 2 and 3 pA events.

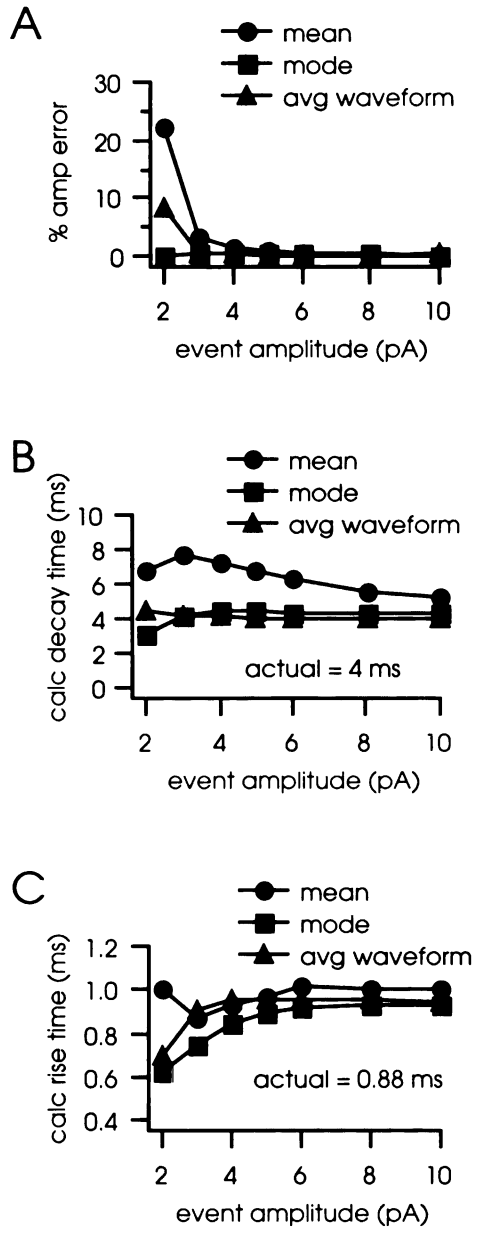
A
mean
mode
avg waveform
% amp error
30
20
10
0
2
4
6
8
10
event amplitude (pA)
B
mean
mode
avg waveform
calc decay time (ms)
10
8
6
4
2
0
actual = 4 ms
2
4
6
8
10
event amplitude (pA)
C
mean
mode
avg waveform
calc rise time (ms)
1.2
1.0
0.8
0.6
0.4
actual = 0.88 ms
2
4
6
8
10
event amplitude (pA)

the program was able to separate the two types of events based solely on kinetics. As an example of this separation, we analyzed a simulated trace containing both fast (amplitude = 5 pA, 10-90% time-to-peak = 0.49 ms, decay = 4 ms) and slow (amplitude = 10 pA, 10-90% time-to-peak = 1.6 ms, decay = 25 ms) events. The resulting bimodal distributions of amplitude, decay time, and rise time give a clear representation of the two different classes of events (Fig 4.7A-C). Finally, Fig 4.7D shows the bimodal distribution of decay time constants resulting from the analysis of an actual recording of synaptic events from a mouse retinal ganglion cell. The separation by kinetics was confirmed by pharmacological experiments in which glutamate receptor antagonists blocked the faster events (less than 6 ms decay time) and antagonists to GABA and glycine receptors blocked the slower events (greater than 6 ms decay time) (Tian et al., 1998).

Fig 4.7: Separation of different populations of events. A simulated trace containing one thousand excitatory (amplitude = 5 pA; 10-90% time-to-peak = 0.49 ms; decay time constant = 4 ms) and one thousand inhibitory events (amplitude = 10 pA; 10-90% time-to-peak = 1.6 ms; decay time constant = 25 ms) was analyzed using a threshold setting of 2 pA and a frequency cut-off of 1000 Hz. A) The amplitude distribution shows a bimodal distribution with peaks at both 5 and 10 pA (marked by arrowheads). B) The decay time constant distribution shows a bimodal distribution with peaks at both 4 ms and 25 ms (marked by arrowheads). The distribution around 4 ms was clearly skewed toward larger values due to the proximity to zero. C) The 10-90% time-to-peak distribution shows a bimodal distribution with peaks at both 0.49 ms and 1.6 ms (marked by arrowheads). D) An actual mouse retinal ganglion cell recording (recorded as described in Tian et al) containing both EPSCs and IPSCs was analyzed using a threshold setting of 2 pA and a frequency cut-off of 1000 Hz. The decay time constant distribution clearly shows a bimodal profile.

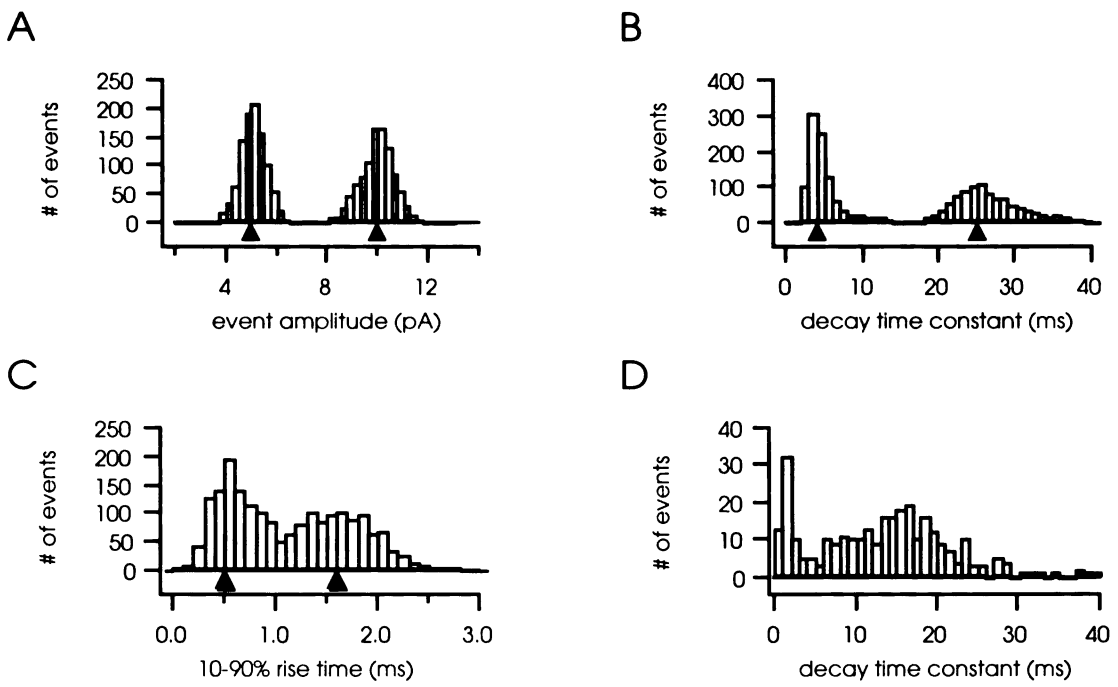
A
# of events
250
200
150
100
50
0
4
8
12
event amplitude (pA)
B
# of events
400
300
200
100
0
0
10
20
30
40
decay time constant (ms)
C
# of events
250
200
150
100
50
0
0.0
1.0
2.0
3.0
10-90% rise time (ms)
D
# of events
40
30
20
10
0
0
10
20
30
40
decay time constant (ms)

Discussion

Our results show that our program can identify events with high sensitivity and a low false positive rate using our event detection program. The program maintained high sensitivity and a low false positive rate even when challenged by events that overlap (Fig 4.4) and events that have different kinetics (Fig 4.5A). Both attributes were required to analyze our recordings of retinal ganglion cells because they often contained overlapping events as well as both fast excitatory and slow inhibitory events (Tian et al., 1998).

The calculated values for the event amplitude, 10-90% time-to-peak, and decay time constant accurately estimated the true values (Fig 4.6A-C). We had three measures for each parameter, namely the mean, the mode, and the average waveform parameters. The mode values and the values derived from the average waveform worked better than the mean although the average waveform values do not work well in the case of multiple event types. The mean worked well for the amplitude and time-to-peak but overestimated the value for the decay time constant. The actual program has additional features that allow a user to discard events that do not have kinetic parameters within a selected range. These criteria allow the isolation of events with particular kinetics from other events.

Our standard approach to using the program on actual data involves determining the standard deviation of an event-free segment of data, which presumably only has noise. Typically, we use a threshold setting of 2.5 to 3 times the standard deviation of the noise. As shown above, the amplitude

criterion can be set as low as 2 times the standard deviation of the noise and still have a low false positive rate; therefore, our choice of threshold is justified. When comparing the frequency of events of different recordings, we use the threshold setting for the trace with the greatest noise for all the traces. In this manner, even though the smaller events may be missed, we can make conclusions about the frequency of events with amplitude greater than a constant threshold. Otherwise, recordings with lower noise might have greater frequency simply because smaller events were detectable in those traces.

In conclusion, this study presents an algorithm that, in essence, only requires the user to input an amplitude criterion in order to detect events with high sensitivity and a low false positive rate. Since detection is based almost completely on a single intuitive parameter, a user can easily optimize the program performance based simply on the noise standard deviation. In addition, the program is relatively insensitive to baseline drifts, overlapping events, and variability in event kinetics and outputs accurate estimates of the amplitude and kinetic parameters of the detected events.

Conclusions

The work in this dissertation presents an approach for analyzing synaptic transmission between cells by first characterizing the spontaneous and quantal synaptic events and then using that information to examine other aspects of synaptic transmission. In particular, we studied multi-quantal neurotransmitter release, light-evoked release functions, light-evoked synaptic terminal vesicle depletion, and the circuitry modulating both light-evoked and spontaneous release. Previously, the work to characterize spontaneous activity was very tedious and time consuming. With the advent of automatic detection software such as the one described here, the characterization has become much more feasible and efficient.

Our results show for the first time that in addition to voltage-gated sodium channels, calcium channels can underlie multi-quantal release from synaptic terminals. This finding was found for both bipolar and amacrine cell release. We propose that calcium action potentials, which have been observed in bipolar cells (Burrone and Lagnado, 1997; Zenisek and Matthews, 1998; Protti et al., 2000), cause relatively large depolarizations in synaptic terminals that cause release from multiple release sites virtually simultaneously a multi-quantal postsynaptic response. Calcium action potentials may serve as an amplification system for voltage responses. Notably, the effect shown in this study may be specific to the L-type calcium channels that are found in both bipolar and amacrine cells. This

type of channel is only found in cells that have the ability to signal through graded potentials rather than sodium spiking.

Our deconvolution method calculated the quantal release function for glutamate, glycine, and GABA. These functions revealed that release even to very strong stimuli only releases a few thousand quanta. In addition, even during the rising phase of the responses, the release is relatively asynchronous. When compared to the anatomical numbers of vesicles in bipolar cell synapses, the quantal release functions also allowed us to evaluate whether bipolar cell synaptic vesicle depletion during light stimulation is likely to occur. Under our condition, we predicted that depletion would not occur. This prediction was supported by results from our pair flash experiments, which shows that very little attenuation is seen in the second response even when separated by only 0.5 seconds from the first response.

Many of the attributes of retinal processing depend on the circuitry of the retinal neurons. We find that a great deal of the spontaneous excitatory input to transient ON/OFF amacrine cells comes from ON-bipolar cells. This may have implications on retinal signaling under different conditions as discussed in Chapter 4. In addition, we find that GABAergic feedback through the $GABA_C$ receptors strongly modulates both the spontaneous and the light-evoked release from both ON- and OFF-bipolar cells. Since light-evoked signals must be distinguished somehow from spontaneous activity, $GABA_C$ receptors may serve as a mechanism to set the level of spontaneous activity so that light-evoked signals can be optimally processed.

References

Ankri, N, et al. (1994). "Automatic detection of spontaneous synaptic responses in central neurons." Journal of Neuroscience Methods **52**(1): 87-100.

Bekkers, JM and Stevens, CF (1989). "NMDA and non-NMDA receptors are co-localized at individual excitatory synapses in cultured rat hippocampus." Nature **341**(6239): 230-3.

Bergman, H and DeLong, MR (1992). "A personal computer-based spike detector and sorter: implementation and evaluation." Journal of Neuroscience Methods **41**(3): 187-97.

Bieda, MC and Copenhagen, DR (2000). "Inhibition is not required for the production of transient spiking responses from retinal ganglion cells." Visual Neuroscience **17**: 243-254.

Burrone, J and Lagnado, L (1997). "Electrical resonance and Ca2+ influx in the synaptic terminal of depolarizing bipolar cells from the goldfish retina." Journal of Physiology **505**(Pt 3)(11): 571-84.

Bykhovskaia, M, et al. (1996). "An algorithm for high-resolution detection of postsynaptic quantal events in extracellular records." Journal of Neuroscience Methods **65**(2): 173-82.

Carlson, CG and Krieger, JW (1996). "A baseline detection method for analyzing transient electrophysiological events." Journal of Neuroscience Methods **67**(2): 211-20.

Clements, JD and Bekkers, JM (1997). "Detection of spontaneous synaptic events with an optimally scaled template." Biophysical Journal **73**(1): 220-9.

Cocatre-Zilgien, JH and Delcomyn, F (1990). "A slope-based approach to spike discrimination in digitized data." Journal of Neuroscience Methods **33**(2-3): 241-9.

Cochran, SL (1993). "Algorithms for detection and measurement of spontaneous events." Journal of Neuroscience Methods **50**(1): 105-21.

Cohen, E and Sterling, P (1990). "Convergence and divergence of cones onto bipolar cells in the central area of cat retina." Philosophical Transactions of the Royal Society of London - Series B: Biological Sciences **330**(1258): 323-8.

Cohen, E and Sterling, P (1991). "Microcircuitry related to the receptive field center of the on-beta ganglion cell." Journal of Neurophysiology **65**(2): 352-9.

Cohen, GA, et al. (1992). "Opioid inhibition of GABA release from presynaptic terminals of rat hippocampal interneurons." Neuron **9**(2): 325-35.

Cook, PB and McReynolds, JS (1998). "Lateral inhibition in the inner retina is important for spatial tuning of ganglion cells." Nature Neuroscience **1**(8): 714-9.

Dempster, J (1993). Computer Analysis of Electrophysiological Signals. London, Academic Press.

Dixon, DB and Copenhagen, DR (1992). "Two types of glutamate receptors differentially excite amacrine cells in the tiger salamander retina." Journal of Physiology **449**: 589-606.

Dong, CJ and Werblin, FS (1998). "Temporal contrast enhancement via GABAC feedback at bipolar terminals in the tiger salamander retina." Journal of Neurophysiology **79**(4): 2171-80.

Edmonds, B and Colquhoun, D (1992). "Rapid decay of averaged single-channel NMDA receptor activations recorded at low agonist concentration." Proceedings of the Royal Society of London. Series B: Biological Sciences **250**(1329): 279-86.

Edmonds, B, et al. (1995). "Mechanisms of activation of glutamate receptors and the time course of excitatory synaptic currents." Annual Review of Physiology **57**(14): 495-519.

Freed, MA and Sterling, P (1988). "The ON-alpha ganglion cell of the cat retina and its presynaptic cell types." Journal of Neuroscience **8**(7): 2303-20.

Frerking, M, et al. (1995). "Variation in GABA mini amplitude is the consequence of variation in transmitter concentration." Neuron **15**(4): 885-95.

Gao, F and Wu, SM (1998). "Characterization of spontaneous inhibitory synaptic currents in salamander retinal ganglion cells." Journal of Neurophysiology **80**(4): 1752-64.

Gao, F and Wu, SM (1999). "Multiple types of spontaneous excitatory synaptic currents in salamander retinal ganglion cells." Brain Research **821**(2): 487-502.

Glantz, SaS, BK (1990). Primer of applied regression and analysis of variance. New York, McGraw-Hill.

Grzywacz, NM, et al. (1998). "Necessity of acetylcholine for retinal directionally selective responses to drifting gratings in rabbit [see comments]." Journal of Physiology **512**(Pt 2): 575-81.

He, S and Masland, RH (1997). "Retinal direction selectivity after targeted laser ablation of starburst amacrine cells." Nature **389**(6649): 378-82.

Hestrin, S, et al. (1990). "Mechanisms generating the time course of dual component excitatory synaptic currents recorded in hippocampal slices." Neuron **5**(3): 247-53.

Hwang, TN and Copenhagen, DR (1999). "Automatic detection, characterization, and discrimination of kinetically distinct spontaneous synaptic events." Journal of Neuroscience Methods **92**(1-2): 65-73.

Kolb, H (1979). "The inner plexiform layer in the retina of the cat: electron microscopic observations." Journal of Neurocytology **8**(3): 295-329.

Lester, RA, et al. (1990). "Channel kinetics determine the time course of NMDA receptor-mediated synaptic currents." Nature **346**(6284): 565-7.

Liu, HH and Kim, YI (1983). "A computer system for real-time data acquisition and analysis of biopotentials and quantal content at the neuromuscular junction." Computer Programs in Biomedicine **16**(3): 161-73.

Lukasiewicz, PD, et al. (1994). "A novel GABA receptor on bipolar cell terminals in the tiger salamander retina." Journal of Neuroscience **14**(3 Pt 1): 1202-12.

Lukasiewicz, PD, et al. (1997). "AMPA-preferring receptors mediate excitatory synaptic inputs to retinal ganglion cells." Journal of Neurophysiology **77**(1): 57-64.

MacNeil, MA and Masland, RH (1998). "Extreme diversity among amacrine cells: implications for function." Neuron **20**(5): 971-82.

Maguire, G, et al. (1989). "Amacrine cell interactions underlying the response to change in the tiger salamander retina." Journal of Neuroscience **9**(2): 726-35.

Man, YH, et al. (2000). "Regulation of AMPA receptor-mediated synaptic transmission by clathrin-dependent receptor internalization." Neuron **25**(3): 649-62.

Manabe, T, et al. (1992). "Postsynaptic contribution to long-term potentiation revealed by the analysis of miniature synaptic currents." Nature **355**(6355): 50-5.

Markram, H, et al. (1998). "Differential signaling via the same axon of neocortical pyramidal neurons." Proceedings of the National Academy of Sciences of the United States of America **95**(9): 5323-8.

Matsui, K, et al. (1998). "Excitatory synaptic transmission in the inner retina: paired recordings of bipolar cells and neurons of the ganglion cell layer." Journal of Neuroscience **18**(12): 4500-10.

Matthews, G (1996). "Neurotransmitter release." Annual Review of Neuroscience **19**(6): 219-33.

McGuire, BA, et al. (1986). "Microcircuitry of beta ganglion cells in cat retina." Journal of Neuroscience **6**(4): 907-18.

Mittman, S, et al. (1990). "Concomitant activation of two types of glutamate receptor mediates excitation of salamander retinal ganglion cells." J. Physiol. **428**: 175-97.

Morales, FR, et al. (1985). "A computerized system for the detection and analysis of spontaneously occurring synaptic potentials." Journal of Neuroscience Methods **13**(1): 19-35.

Nirenberg, S and Meister, M (1997). "The light response of retinal ganglion cells is truncated by a displaced amacrine circuit." Neuron **18**(4): 637-50.

Oghalai, JS, et al. (1994). "A neural network-based spike discriminator." Journal of Neuroscience Methods **54**(1): 9-22.

Otis, TS, et al. (1991). "Perpetual inhibitory activity in mammalian brain slices generated by spontaneous GABA release." Brain Research **545**(1-2): 142-50.

Partin, KM, et al. (1993). "Selective modulation of desensitization at AMPA versus kainate receptors by cyclothiazide and concanavalin A." Neuron **11**(6): 1069-82.

Protti, DA, et al. (2000). "Light evokes Ca2+ spikes in the axon terminal of a retinal bipolar cell [see comments]." Neuron **25**(1): 215-27.

Rall, W (1969). "Time constants and electrotonic length of membrane cylinders and neurons." Biophysical Journal **9**(12): 1483-508.

Rorig, B and Grantyn, R (1993). "Glutamatergic and GABAergic synaptic currents in ganglion cells from isolated retinae of pigmented rats during postnatal development." Brain Research. Developmental Brain Research **74**(1): 98-110.

Roska, B, et al. (1998). "Response to change is facilitated by a three-neuron disinhibitory pathway in the tiger salamander retina." Journal of Neuroscience **18**(9): 3451-9.

Salganicoff, M, et al. (1988). "Unsupervised waveform classification for multi-neuron recordings: a real-time, software-based system. I. Algorithms and implementation." Journal of Neuroscience Methods **25**(3): 181-7.

Shen, Y, et al. (1999). "Characterization of AMPA receptors on isolated amacrine-like cells in carp retina." European Journal of Neuroscience **11**(12): 4233-40.

Silver, RA, et al. (1996). "Deactivation and desensitization of non-NMDA receptors in patches and the time course of EPSCs in rat cerebellar granule cells [published erratum appears in J Physiol (Lond) 1996 Nov 1;496(Pt 3):891]." Journal of Physiology **493**(Pt 1)(6): 167-73.

Taylor, WR, et al. (1995). "Characterization of spontaneous excitatory synaptic currents in salamander retinal ganglion cells." Journal of Physiology **486**(Pt 1): 207-21.

Thibos, LN and Werblin, FS (1978). "The properties of surround antagonism elicited by spinning windmill patterns in the mudpuppy retina." Journal of Physiology **278**(3): 101-16.

Tian, N, et al. (1998). "Analysis of excitatory and inhibitory spontaneous synaptic activity in mouse retinal ganglion cells." Journal of Neurophysiology **80**(3): 1327-40.

Tian, N and Slaughter, MM (1995). "Functional properties of a metabotropic glutamate receptor at dendritic synapses of ON bipolar cells in the amphibian retina." Visual Neuroscience **12**(4): 755-65.

Tovar, KR and Westbrook, GL (1999). "Mobile NMDA receptors contribute to the NMDA receptor-mediated EPSC." Society for Neuroscience Abstracts **25**: 470.

Tran, MN, et al. (1999). "AMPA receptor kinetics limit retinal amacrine cell excitatory synaptic responses." Visual Neuroscience **16**(5): 835-42.

Turrigiano, GG (2000). "AMPA receptors unbound: membrane cycling and synaptic plasticity." Neuron **26**(1): 5-8.

Turrigiano, GG, et al. (1998). "Activity-dependent scaling of quantal amplitude in neocortical neurons [see comments]." Nature **391**(6670): 892-6.

von Gersdorff, H and Matthews, G (1994). "Dynamics of synaptic vesicle fusion and membrane retrieval in synaptic terminals [see comments]." Nature **367**(6465): 735-9.

von Gersdorff, H and Matthews, G (1997). "Depletion and replenishment of vesicle pools at a ribbon-type synaptic terminal." Journal of Neuroscience **17**(6): 1919-27.

von Gersdorff, H, et al. (1996). "Evidence that vesicles on the synaptic ribbon of retinal bipolar neurons can be rapidly released." Neuron **16**(6): 1221-7.

Werblin, F, et al. (1988). "Neural interactions mediating the detection of motion in the retina of the tiger salamander." Visual Neuroscience **1**(3): 317-29.

Werblin, FS (1972). "Lateral interactions at inner plexiform layer of vertebrate retina: antagonistic responses to change." Science **175**(25): 1008-10.

Werblin, FS and Copenhagen, DR (1974). "Control of retinal sensitivity. 3. Lateral interactions at the inner plexiform layer." Journal of General Physiology **63**(1): 88-110.

Wong, LA and Mayer, ML (1993). "Differential modulation by cyclothiazide and concanavalin A of desensitization at native alpha-amino-3-hydroxy-5-methyl-4-isoxazolepropionic acid- and kainate-preferring glutamate receptors." Molecular Pharmacology **44**(3): 504-10.

Wu, SM (1987). "Synaptic connections between neurons in living slices of the larval tiger salamander retina." Journal of Neuroscience Methods **20**(2): 139-49.

Yamada, S, et al. (1992). "Data processing for multi-channel optical recording: action potential detection by neural network." Journal of Neuroscience Methods **43**(1): 23-33.

Yang, XW and Shamma, SA (1988). "A totally automated system for the detection and classification of neural spikes." Ieee Transactions on Biomedical Engineering **35**(10): 806-16.

Zenisek, D and Matthews, G (1998). "Calcium action potentials in retinal bipolar neurons." Visual Neuroscience **15**(1): 69-75.

Zhang, J, et al. (1997). "Serial inhibitory synapses in retina." Visual Neuroscience **14**(3): 553-63.